Study of crystallinity and piezoelectric properties of KNNS-BZ-BKH ceramics for Energy Harvesting

環境発電に向けた KNNS-BZ-BKH セラミックの結晶性と圧電特性の研究

2022 年 3 月

曽 理浩雯

Study of crystallinity and piezoelectric properties of KNNS-BZ-BKH ceramics for Energy Harvesting

環境発電に向けた KNNS-BZ-BKH セラミックの

結晶性と圧電特性の研究

弘前大学大学院理工学研究科

博士後期課程

博士論文

2022 年 3 月

曽 理浩雯

Study of crystallinity and piezoelectric properties of KNNS-BZ-BKH ceramics for Energy Harvesting

環境発電に向けた KNNS-BZ-BKH セラミックの結晶性と圧電特性の研究

Table of Contents

Abstract 6

Acknowledgments 8

1. Introduction 9

1.1 Energy harvesting overview 9

1.1.1 Batteries 10

1.1.2 Capacitors 12

1.1.3 Solar energy 13

1.1.4 Heat-Thermo 15

1.1.5 Vibration 17

1.2 Piezoelectric Materials 18

2. Lead-Free KNN-Based (KNNS-BZ-BKH) 23

2.1 Background 23

2.1.1 Manifestations of piezoelectric properties: 23

2.1.2 Piezoelectric and related parameters 25

2.1.3 The main factors affecting the frequency effect 25

2.1.4 Phase transition 25

2.1.5 Microstructure 29

2.2 Production Methods 31

2.2.1 Powder production 31

2.2.2 Polyvinyl alcohol 32

2.2.2 Sintering process 32

2.3 Research Work objectives 35

3. Experimental Procedure 35

3.1 Materials Selection 35

3.1.1 Perovskite 36

3.1.2 (K, Na) NbO3 38

3.2 Samples Preparation 40

3.2.1 Powder preparation 40

3.2.2 Conventional solid-state reaction 40

3.2.3 Pellet experiment 42

3.3 Analysis Methods 50

3.3.1 X-ray Diffraction 50

3.3.2 Scanning electron microscope 51
3.3.3 Energy Dispersive X-ray Spectroscopy 51
4. Results and Discussion 53
4.1 Structural Evaluation 53
4.1.1 XRD analysis of powder 53
4.2 Morphology analysis 56
4.2.1 SEM analysis of powder 56
4.3 Composition Analysis 57
4.3.1 XRD analysis of powder 57
4.3.2 EDS analysis of powder 60
4.4 Result of the properties of the pellet 66
4.4.1 Density and d_{33} measurement of pellet 66
5. Conclusion 68
5.1 Summary 68
5.2 Perspectives 68

Abstract

In order to study how to improve the crystallinity and precise composition of (K, Na) (Nb, Sb) O_3-based piezoelectric materials in lead-free piezoelectric material, this article explains the following main objective:

- Element control of (K, Na) (Nb, Sb) O_3-based lead-free piezoelectric materials
- Optimization of sintering temperatures for (K, Na) (Nb, Sb) O_3-based lead-free piezoelectric materials
- Production of (K, Na) (Nb, Sb) O_3-based lead-free piezoelectric material pellets

This thesis contains five chapters as follows:

Chapter 1 describes the attractive function of piezoelectric materials as general background. Pb (Zr, Ti)O_3 (PZT) materials are among the most important for piezoelectric applications, such as actuators, sensors, and energy harvesting. However, in recent years, the pressure of environmental protection and the EU RoHS (The Restriction of Hazardous Substances Directive) regulations have all put forward requirements for lead-free piezoelectric materials. (K, Na) (Nb, Sb) O_3-based piezoelectric materials have become one of the most promising lead-free piezoelectric materials due to their huge d_{33} and excellent electrical properties. The current research on (K, Na) (Nb, Sb) O_3-based piezoelectric materials mainly focuses on the influence of various additives on the phase transition temperature and electrical properties.

Chapter 2 describes the purpose and aim of this study to investigate (K, Na) (Nb, Sb) O_3-based lead-free piezoelectric materials.

Chapter 3 introduces the research direction of (K, Na) NbO_3-based lead-free piezoelectric materials, describes the production process, and analysis of the (K, Na) (Nb, Sb) O_3-based piezoelectric materials, including the process from starting powders to polarized pellets to estimate the piezoelectric properties. The two o main experimental procedures of this study were discussed as follows: First, the powder experiment includes the analysis and control of the composition of the material; Second, the pellet experiment includes the control of sintering and polarization process, X-ray powder diffraction, and Scanning electron microscope /Energy-dispersive X-ray spectroscopy were used for analysis in both experimental processes.

Chapter 4 discusses the experimental results, compares the X-ray powder diffraction results of powder samples under different heating program patterns, X-ray powder diffraction results of powder samples under different mol% K, and compares the X-ray powder diffraction results and electrical properties pellet samples under different mol% K.

Finally, the conclusion summarizes the experimental results and discusses the research direction of optimizing the crystal structure and electrical properties of (K, Na) (Nb, Sb) O_3-based piezoelectric ceramics.

Acknowledgments

I did my Ph.D. within functional creation science in the Graduate School of Science and Engineering, Hirosaki University.

I would like to thank my mentor and supervisor, Professor Kenji Itaka from Hirosaki University. A special thanks to the North Japan Research Institute For Sustainable Energy (NJRISE) director for giving me such a precious opportunity to obtain a Ph.D. from Hirosaki University.

Again a special Thanks to Professor Kenji Itaka for his encouragement, supervising, and guidance during my studies. I must sincerely admit that at the beginning of my PhD study, I did not have the proper scientific research attitude and mentality that a scientific researcher should have. Professor Kenji did not give up on me. He continued to urge me, motivate me, and guide me. I was able to acquire this knowledge in lead-free piezoelectric ceramic materials, mainly due to the hard teaching of Kenji Itaka.

Thanks to Professor Honda, Professor Guan, Professor Kubota, Professor Ioka, and Professor Yoshida of the Institute for their selfless help. Thank you very much for your guidance and help to me!

During my doctoral course, I am incredibly grateful to my predecessor Dr. Rabie Benioub for his selfless help, which helped me establish a correct research attitude and guided my research and shared ideas. The method has benefited me a lot. It is a great honor for me to have the opportunity to learn from him. In addition to our group members' support, Boucetta Abderahmane and Chahtou Amina gave me tremendous help.

In studying for a degree, the Yoneyama Award Society has also given me tremendous help, not only economically, but also culturally, and ideologically, allowing me to have more in-depth contact with Japanese society and understand Japanese customs. I live in a foreign land but can feel the warmth of relatives and friends. I am grateful to the teachers, classmates, and friends from all countries and regions who have contacted and exchanged in Hirosaki and Aomori city. I feel a lot about the contacts and exchanges. Thank you very much for your support and help!

Finally, I want to thank my parents, my brothers and sisters, for various reasons, it is not convenient to return to China in recent years. I owe them when I want to be with my family, but they still firmly support me and encourage me. My family's support for me has crossed the physical barriers; thank you very much!

1. Introduction

1.1 Energy harvesting overview

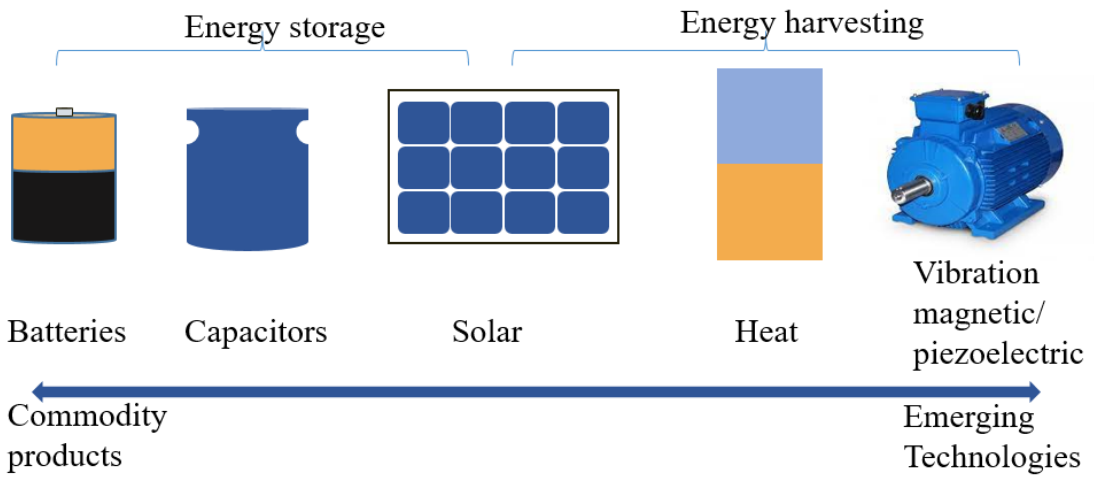

Fig. 1 Conventional Energy Storage vs. Emerging Energy HarvestinFig 1.

Energy harvesting is a type of small wireless device (such as wearable electronic devices and devices in wireless sensor networks) that are available but not used in the surrounding environment (such as solar energy, thermal energy, wind energy, salinity gradient, and kinetic energy). Technology for storing electrical energy [1]. Portable power supply applications are about a few $\mu W/cm^3$, and mechanically powered generators are hundreds of $\mu W/cm^3$ [2]. Although, in principle, this technology is similar to large-scale renewable energy power generation such as wind turbines, the energy collected by energy harvesting is much smaller, usually tens of microwatts to several watts. Nevertheless, relative to battery-powered systems, energy harvesting is an attractive alternative. Some systems that require long-term use, low power consumption, need to be self-sustaining, or some inconvenient applications to use batteries, such as sensor networks or remote systems that are inconvenient to access, and battery handling is also an environmental issue. Because of the above reasons, energy harvesting technology has a bright future. The continuous development of energy harvesting technology is based on the following theory: The device collects energy from the environment in real-time and uses it immediately. The collected energy does not need to be stored for a long time, which in theory dramatically extends the service life of the equipment.

Energy harvesting has received increasing attention in self-contained wireless electronic devices, remote sensors, and portable devices in the past few decades. For example, a transducer designed

on the principle of electromagnetic induction defined by Faraday's law can be used as an energy harvester. Piezoelectric energy harvester technology is becoming more and more mature. So far, energy harvesting technology has focused on kinetic energy (vibration or motion), thermal gradients, or incident light.

The energy harvesting performance is greatly affected by the amount and nature of the original energy in the environment. Before designing an energy harvesting solution, the application constraints and energy parameters must be considered. Energy harvesting has also introduced a series of new challenges, most of which can be attributed to environmental energy being neither controllable nor predictable. The potential for energy harvesting largely depends on the specific properties of the material. This chapter reviews the essential characteristics and potentials of materials used for energy harvesting, introduces the concept of energy harvesting, discusses the latest technology of materials used for energy harvesting such as piezoelectric, photovoltaic, thermoelectric, electromagnetic, and focuses on the materials used. And related features.

1.1.1 Batteries

1.1.1.1 Alkaline battery

As an energy storage device, alkaline batteries refer to batteries that use alkaline electrolytes. The electrode materials used in alkaline batteries include zinc-manganese dioxide, zinc-mercury oxide, cadmium-nickel hydroxide, etc. In life, standard alkaline batteries are alkaline zinc-manganese batteries with manganese dioxide as the battery cathode, zinc as the anode, and potassium hydroxide aqueous solution as the electrolyte. Because the utilization rate of electrode materials is improved, the purity and density of manganese dioxide used in the cathode and zinc powder used in the anode have reduced the volume of internal parts. Alkaline batteries generally have 3 to 6 times more capacity than carbon-zinc batteries.

Alkaline batteries account for 80% of the US market, and global production exceeds 10 billion. In Japan, alkaline batteries account for 46% of the market. Alkaline batteries account for 68% of the market in Switzerland, 60% in the UK, and 47% in the European Union, including secondary batteries [3-7].

Alkaline batteries may leak electrolytes containing potassium hydroxide if left unused for a long time, which may cause irritation to the eyes, respiratory tract and skin, and may cause blindness; it may also corrode metals and damage electronic parts. Although they are storage batteries, alkaline batteries are primarily designed for one-time use. Forced charging may cause the battery

to rupture and corrosive electrolyte leakage. Keep the environment dry and suitable temperature during storage. Excessive temperature will also cause the battery to rupture and electrolyte leakage and shorten the battery's shelf life. The mercury, heavy metals, and corrosive chemicals in old alkaline batteries are still challenging to dispose of today. Alkaline batteries in Europe cannot be discarded with household garbage and need to be recycled by stores where the batteries are sold. In the United States, California requires the recycling of all alkaline batteries. Vermont also has a statewide alkaline battery collection plan [8].

1.1.1.2 Lithium battery

Lithium batteries use lithium metal or lithium alloy as the anode material and use a non-aqueous electrolyte solution. Different from rechargeable lithium-ion batteries, lithium batteries generally refer to disposable batteries [9]. Lithium ions can move between the anode and the cathode, using a lithium compound as the cathode material. Pure lithium has exceptionally high activity and can even react with moisture in the air. Lithium-ion batteries use low-activity lithium compounds. Lithium batteries account for 28% of the Japanese market but only 1% of the Swiss market. Only 0.5% of all sales, including secondary batteries, are lithium primaries in the European Union [10-13].

Lithium batteries are widely used in portable electronic devices and require 0.15 to 0.3 kilograms of lithium per kilowatt-hour. Lithium batteries can be used in many vital devices that require long-term use, such as pacemakers or other implantable electronic medical devices. The service life of lithium iodide batteries specially designed for these devices can reach more than 15 years. Lithium batteries can replace ordinary alkaline batteries in many scenarios, such as clocks and cameras. Although lithium batteries are more expensive, long-life lithium batteries can reduce the frequency of battery replacement. Lithium batteries are also used in oceanography. The cost of remote marine instruments is higher, and it is more reasonable to use high-capacity lithium batteries. Portable electronic devices have strong demand for small lithium batteries, such as personal digital assistants, watches, cameras, thermometers, remote control car locks, etc. Lithium batteries can meet the short-term, high-current requirements of these devices. Lithium batteries can maintain a higher voltage for a longer period than alkaline batteries.

Lithium batteries can provide extremely high currents and can discharge very quickly in a short circuit. This is useful in high-current applications, but discharging too fast in a cobalt-containing battery will cause the battery to overheat, reduce the resistance of the cobalt-containing material,

and cause the battery to rupture or even explode. Lithium thionic chloride batteries are prone to such problems and are often prevented by overheating protection or vents. Due to the above risks, the transportation of lithium batteries is prohibited under certain circumstances, especially air transportation.

1.1.2 Capacitors

Capacitors are passive electronic components that store computers in an electric field. The energy storage performance can be expressed in terms of capacitance. There is the capacitance between adjacent conductors in the circuit, and the capacitor is an electronic component added to increase the capacitance in the circuit [14].

In October 1745, Ewald Georg von Kleist of Pomerania, Germany, discovered that by connecting a high-voltage electrostatic generator to a specific volume of water in a hand-held glass jar through a wire, an electrical charge could be stored. The following year, the Dutch physicist Pieter van Musschenbroek invented a similar capacitor named as the Leiden Jar after the University of Leiden [15,16].

Capacitors have different shapes and structures. Commonly used capacitors have at least two metal plates or conductor plates, and the middle is filled with dielectric. The conductor can be metal foil, film, sintered electrolyte, or electrolyte. Non-conductive dielectrics can increase the storage capacity of capacitors. Common media include glass, ceramics, plastic film, paper, mica, and oxides. Capacitors are in great demand in the circuit technology, and when they are different from resistors, ideal capacitors do not consume energy. When a dielectric separates a voltage between conductors, an electric field will be generated on the dielectric. The capacitance of a capacitor is defined as the ratio between the accumulated charge and the conductor voltage. The capacitance of a capacitor is proportional to the conductor's surface area and inversely proportional to the distance between the conductors. The dielectric between the conductors will generate a small leakage current, and there is an upper limit to the electric field strength that the dielectric can withstand so that the capacitor will have a breakdown voltage. The conductor and its pins in the capacitor will produce additional equivalent series inductance and equivalent series resistance.

Capacitors are often used to block direct current in circuits, and alternating current can flow through the capacitor. In the analog filter circuit, the capacitor can smooth the power output. The capacitor and inductor in the resonant circuit can tune the radio to a specific frequency. Capacitors in power transmission systems can stabilize voltage and power.

A capacitor consists of two electrodes. The charge stored on the two electrodes is equal in magnitude and opposite in sign. The electrode usually uses an aluminum sheet or aluminum foil. Electrolytic capacitors usually use alumina as the dielectric. The charge is stored on the surface of the electrode near the dielectric. Since the charges stored in the two electrodes are equal in magnitude but opposite in sign, the capacitor remains electrically neutral.

The capacitance of some capacitors will decrease as the components age. The dielectric deterioration causes a decrease in the capacity of ceramic capacitors. The type of dielectric, the ambient temperature, and the storage temperature will all affect the aging, and the working voltage has a relatively small effect on the deterioration of the capacitor. Component aging can be alleviated by heating the component past the Curie point. The component ages rapidly when it first works, and the electrolytic capacitor will age as the electrolyte evaporates. Capacitors that store energy can be used as batteries to provide short-term power. Capacitors often provide power when replacing batteries to prevent stored data from disappearing due to power failure. Capacitors can also be used to moderate the output of a full-bridge or half-bridge rectifier in the power supply. It can also store energy in the capacitor pump circuit to provide higher than the input voltage.
Because the capacitor can block and filter the direct current signal, it is called alternating current coupling. The capacitor in this application scenario will have a larger capacitance. The energy stored in the capacitor can be used to express information, and the capacitor can act as an integrator in an analog circuit. Capacitors can also be used for sensing applications to measure air humidity. Capacitors that work under high voltage and high currents are extremely dangerous. When the voltage exceeds the limited value of the capacitor, it may cause damage. The failure of the insulating material may cause the insulating liquid to evaporate, causing the capacitor to swell, rupture, or even explode. Capacitors working in a robust current environment for a long time will overheat, and the accumulated heat may damage the capacitors.

1.1.3 Solar energy

Solar energy includes the light and heat radiated by the sun. The technical facilities that use solar energy include solar collectors, solar photovoltaic power generation, solar thermal power generation, and artificial photosynthesis. According to the method of capture and distribution, solar energy technology is divided into passive and active solar energy. ‘Passive’ includes building orientation and material selection; ‘active’ include photovoltaic and thermal energy utilization systems.

The earth received solar radiation of 174PW (peat watts) [17]. About 30% of the solar energy is reflected in space, and clouds, oceans, and land absorb the rest. The solar spectrum on the earth's surface includes a small portion of near-ultraviolet, all visible light, and near-infrared. The solar energy absorbed by the atmosphere, ocean, and land is about 38.5 million EJ per year, and the solar energy absorbed per hour is even more than the energy used in the whole world in 2002 [18,19]. Through photosynthesis, biomass is stored at about 3850 EJ per year [20], and the existing biomass energy potential is more than 100-300 EJ per year. The solar energy reaching the earth in a year exceeds twice the energy obtained by human beings from all non-renewable resources. Factors such as geography, time, clouds, and land limit the number of solar energy humans can use. Areas close to the equator enjoy a higher amount of solar radiation. There is no solar radiation on the surface at night, and the clouds will block incident light. The land also has a significant influence on the use of solar energy. For example, the roof is an ideal place to use solar panels. Except for geothermal energy and tidal energy, all other renewable energy sources are derived from the sun. The methods of using solar energy are:

1) Photoelectric conversion, using solar cells to obtain electricity
2) Use mirrors to reflect sunlight to solar cells (reduce power generation costs)
3) Solar water heater
4) Adsorption refrigeration
5) Solar heating
6) Solar public facilities

Photovoltaic and concentrating solar energy can be used to convert solar energy into electricity. Photovoltaic cells use the photovoltaic effect to convert light into electric current. Concentrating solar power systems use lenses or mirrors to focus large areas of sunlight into small beams. Photovoltaic uses semiconductor materials with a photovoltaic effect to convert light into electrical energy. The photovoltaic effect is commercially applied to power generation and photoelectric sensors. Photovoltaic systems include multiple solar cells that generate electricity. Photovoltaic devices can be installed on the ground, roof, wall, etc. The advantages of photovoltaic systems are: operation does not produce pollution and greenhouse gases, and silicon is widely present in the earth's crust. Solar thermal energy can be used in water heating, space heating, cooling, and other fields. In mid-latitude areas, solar thermal systems can increase the water temperature to 60 degrees Celsius [21]. The most common solar water heaters are evacuated tube collectors and glass flat

plate collectors, often used for domestic water, while unglazed plastic collectors are mainly used in swimming pool heating.

With the development of science and technology and investment in research and development, the cost of solar panels continues to decline, but the high investment in the initial stage of investment limits the promotion of this technology. Considering factors such as climate, sunshine intensity, investment return ratio and other factors, solar energy systems are not suitable for all corners of the world. The rainy days in some areas and the length of sunshine limit solar energy systems. The design of solar power plants needs to consider the impact on ecology and the environment. The silicon, germanium, boron, etc., used in the production of solar panels must be handled carefully to prevent environmental pollution.

1.1.4 Heat-Thermo

The thermoelectric effect refers to using thermocouples to convert temperature differences into voltage and vice versa [22]. First discovered in 1794 by Italian scientist Alessandro Volta [23]. When the temperature on both sides of the thermocouple differs, the hot spot device generates a voltage. On the atomic scale, the temperature barrier causes the charge carriers in the material to diffuse from the hot side to the cold side.

As a branch of the research field of organic semiconductors, thermoelectricity is currently receiving wide attention. Thermoelectric research focuses on developing lightweight, flexible and inexpensive components as an alternative power source to generate electricity from thermal gradients. Thermoelectric generators can directly convert heat into electrical energy without moving parts, run long, and work even with small heat sources and slight temperature differences. These characteristics make thermoelectric technology very attractive.

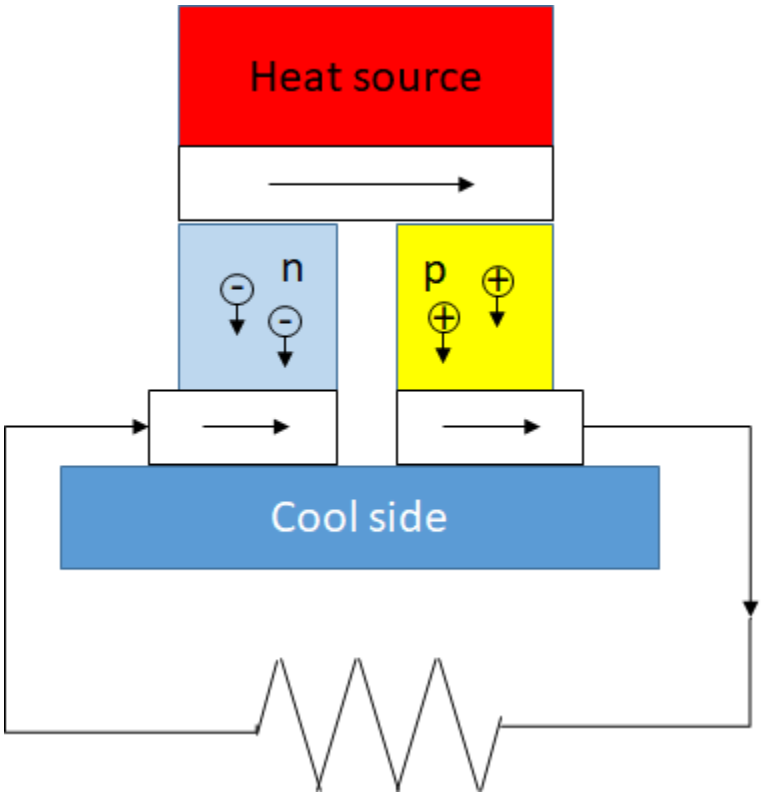

Fig. 2 thermoelectric generators

In order to meet the needs of thermoelectric generators, the thermoelectric materials used need to have good electrical conductivity and low thermal conductivity. Three types of semiconductors, bismuth telluride (Bi_2Te_3), lead telluride (PbTe), and silicon-germanium (SiGe), can meet these requirements. The thermoelectric module includes two different thermoelectric bodies, and n-type and p-type semiconductor materials are connected at the ends of the two thermoelectric bodies. The temperature difference between the two ends generates a direct current, and the current intensity is proportional to the temperature difference. The thermoelectric generator module faces a long-term working environment with high thermal stress and strain, prone to mechanical fatigue. The strength of the node and the choice of material are of great importance. The efficiency of thermoelectric modules is greatly affected by design. For example, thermoelectric materials should be thermally connected in parallel and electrically connected in series. Although the thermoelectric module has no moving parts to avoid friction loss, the thermoelectric generator is still inefficient. However, thermoelectric power generation can be applied to waste heat environments and can be used as a powerful supplement to other energy sources. Since the direction of heating and cooling is affected by the applied voltage, thermoelectric devices can also be used for temperature control. Such as thermoelectric refrigeration, which generates a temperature difference in two circuits with

different electrical conductors by applying current. The advantages of thermoelectric refrigeration are stable operation, no noise, no vibration, and no gas emissions. Solar-powered refrigerators are excellent in mobility and robustness and do not require regular maintenance.

In the past few decades, thermoelectric materilas have made significant progress. These advances are reflected in processing and characterization techniques and new theories generated during the research process. Thermoelectric technology has been widely used in military, aerospace, medical, and waste heat utilization fields. In the future, thermoelectric materials with higher heat transfer efficiency and lower contact resistance will further promote the research and development of thermoelectric technology.

1.1.5 Vibration

Vibration energy harvesting refers to the conversion of vibration energy into electrical energy. It can be achieved by electromagnetic induction or piezoelectric fibers.

Vibration is almost everywhere: in cars, airplanes, trains, bicycles, washing machines, bridges, volcanoes, etc. Although these vibrations' frequency distribution and amplitude are different, it is possible to use appropriate energy harvesters to cooperate with different sources. Good coordination is the foundation because it improves the environmental energy transfer rate, which means that the mechanical impedance of the system must match the mechanical impedance of the vibration source.

1.1.5.1 Vibration-Magnetic

Vibration power generators can convert the kinetic energy of vibration into electrical energy. The vibration may come from sound pressure waves or other environmental vibrations. The resonator amplifies the vibration source, and the transducer that converts the vibration energy into electrical energy can form a vibration generator. The transducer can be constructed using magnets or coils. An electromagnetic generator designed based on Faraday's law of induction converts vibration energy into electrical energy. The vibration will cause the distance between the magnet and the coil to change, the magnetic flux changes, and electromagnetic force is generated. The coil is usually made of diamagnetic material. Compared with piezoelectric generators, this generator can provide more power.

1.1.5.2 Vibration-Piezoelectric

Piezoelectricity refers to applying mechanical stress to certain solid materials to cause the accumulation of electric charges in the solid materials. The term piezoelectric refers to electricity generated by pressure and latent heat. The piezoelectric effect is caused by a crystal material's linear electromechanical interaction between mechanical energy and electrical energy without rotation symmetry [24]. The piezoelectric effect is a reversible process, and materials with the piezoelectric effect also have an inverse piezoelectric effect: the internal mechanical strain is caused by applying an external electric field. The inverse piezoelectric effect can be applied to ultrasound. The piezoelectric effect has been applied to inkjet printing, sound and detection, high-voltage electricity generation, and micro balance. The fundamental component of a scanning needle microscope is that it can resolve images on the atomic scale. It can also be used in heating equipment, flashlights, and cigarette lighters daily.

1.2 Piezoelectric Materials

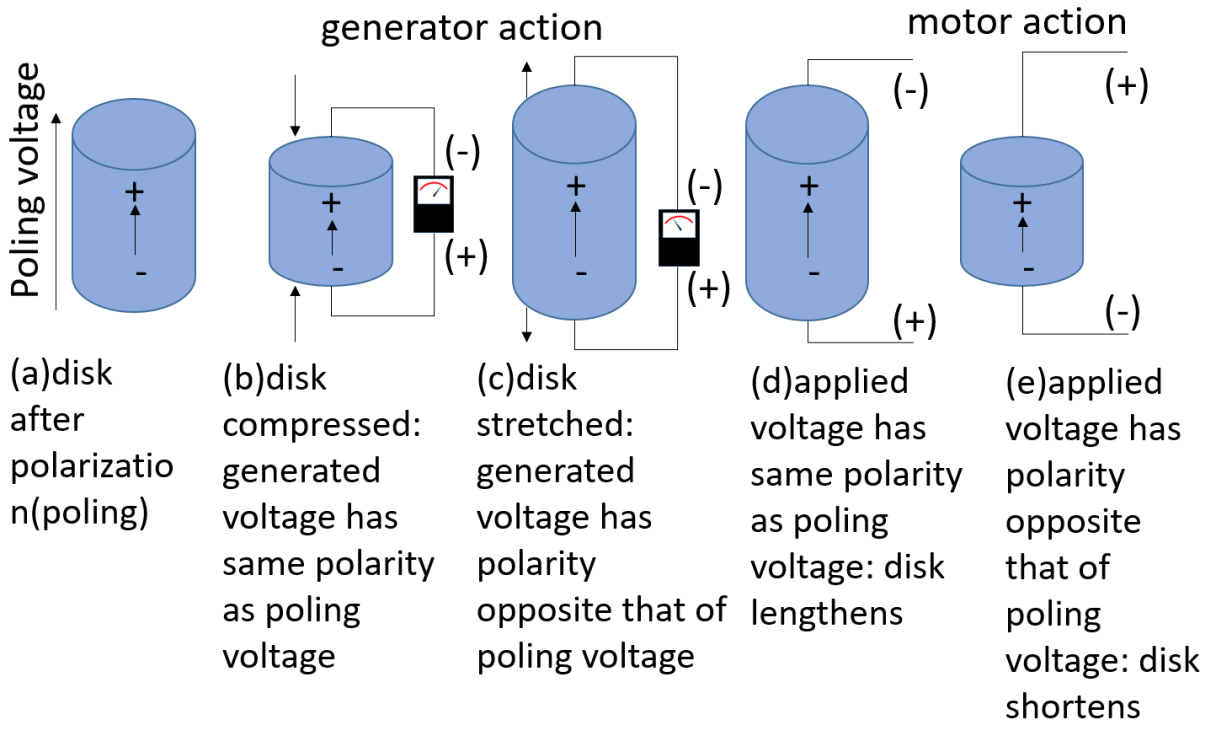

Fig. 3 Description of Piezoelectric Ceramics Principle

The piezoelectric effect is closely related to the electric dipole moment. Ions induce the electric dipole moment on the lattice sites in an asymmetric charge environment or molecular groups.

Consider each dipole as a vector, and multiple dipoles form a dipole density vector field P. The directions of similar dipoles in the Weiss domain tend to be the same. Typically, the domain orientation is random, but a polarization process can align the domains. Polarization is a process of applying a strong electric field on a material, usually in a high-temperature environment, but not all piezoelectric materials can be polarized. What has a significant impact on the piezoelectric effect is the change in the polarization intensity, polarization direction, or both caused by the reconfiguration of the dipole when the material is subjected to mechanical stress. The change depends on 1) the polarization direction within the crystal, 2) the symmetry, and 3) the mechanical stress applied. Polarization changes are manifested as changes in the surface charge density of crystal planes.

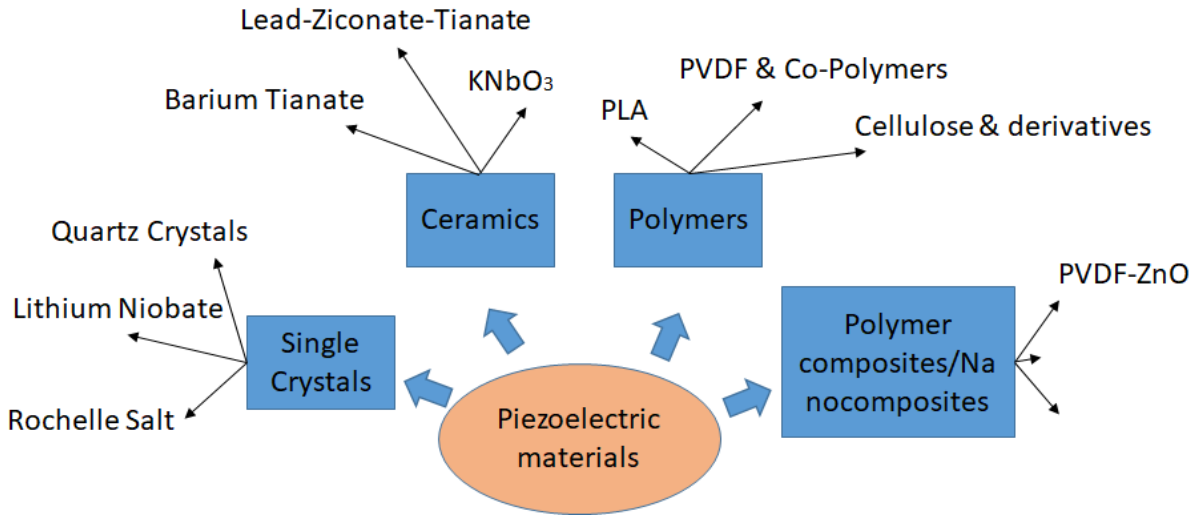

Fig. 4 Different Classes of piezoelectric Materials

Piezoelectric material is a material with a non-centrosymmetric crystal structure. When the material is deformed by external stress, the internal anions and cations will be displaced, resulting in surface charges. Piezoelectric materials can be roughly divided into crystals, ceramics, and polymers. Quartz is the most widely used single crystal piezoelectric material. Naturally produced quartz can be used in equipment after the strict screening. Single crystal piezoelectric materials can be manufactured by various methods, such as aqueous solution growth, the Czochralski method, and gas-phase reaction growth. Single crystal quartz is generally prepared using hydrothermal technology. Among various piezoelectric materials, piezoelectric ceramic, an artificial polycrystalline piezoelectric material composed of multiple ferroelectric particles,

exhibits macroscopic piezoelectricity after being subjected to an external electric field plan. Compared with natural quartz, piezoelectric ceramics have a higher piezoelectric constant and lower cost. The most commonly used piezoelectric ceramics are lead zirconate titanate, barium titanate, and lead titanate. Compared with single-crystal materials, inorganic ceramic piezoelectric materials are not restricted by the crystal direction and are easier to manufacture into various shapes and sizes. Organic polymer piezoelectric materials have lower Young's modulus and higher piezoelectric stress constant than inorganic piezoelectric materials and are more suitable for sensors. Piezoelectric polymers can be made into larger areas and more flexible cutting sensors and actuators. Piezoelectric materials can be used in electronic devices such as actuators, sensors, accelerators, ultrasonic motors, and transducers. Lead-Zirconate-Titanate ceramics are famous among various piezoelectric materials because of their high sensitivity and high g_{33} value. However, this type of ceramic has a low Curie temperature and cannot be widely used in harsh environments. One of the solutions is to integrate it into industrial appliances made of plastic. One of the development directions is the large-scale integration of piezoelectric composite materials through thermal welding or complaint processes.

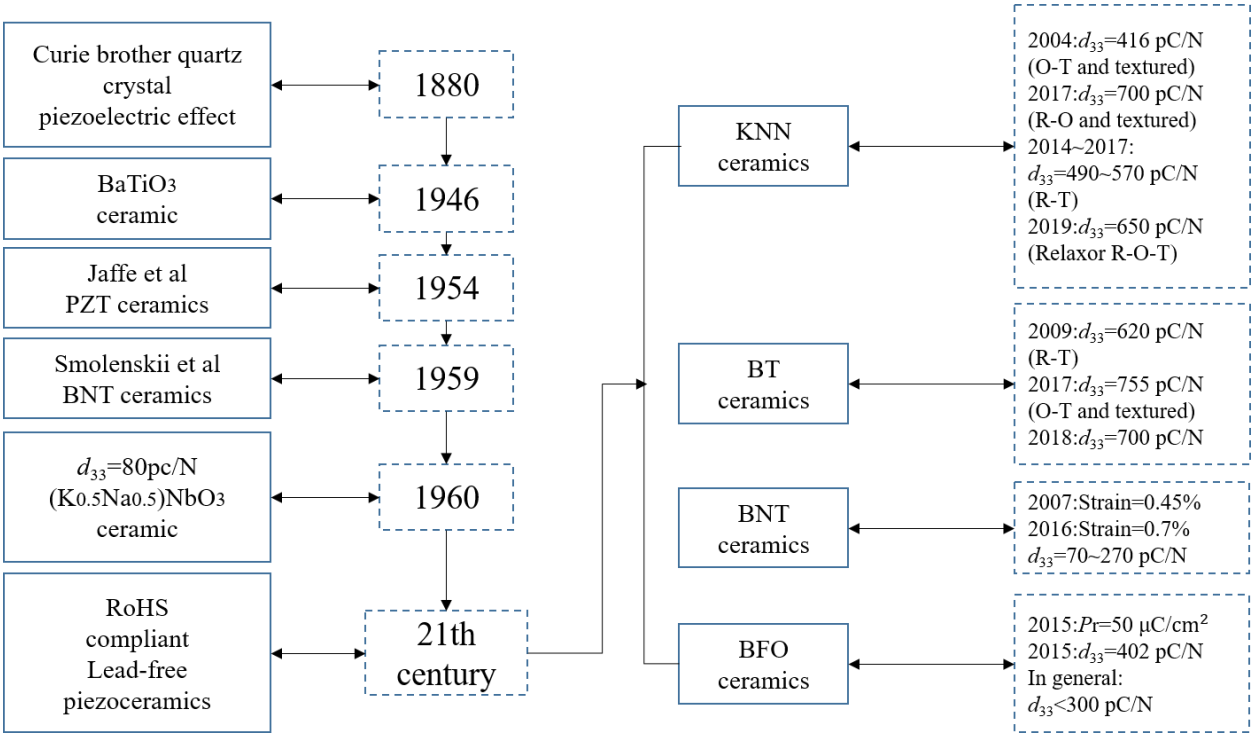

Fig. 5 Lead-free piezoelectric Materials History

In 1880, the brothers Pierre Curie and Jacques Curie demonstrated the direct piezoelectric effect for the first time [25]. They combined the existing thermoelectric knowledge and understanding

of the potential crystal structure to generate thermoelectricity, predicted the crystal behavior, and used tourmaline, quartz, and other crystal experiments to prove the piezoelectricity. In 1881, Gabriel Lippmann mathematically deduced the inverse piezoelectric effect based on the basic thermodynamic principles, and the Curies experiment confirmed the inverse piezoelectric effect [26]. BaTiO3 is still the most widely used ferroelectric material 60 years after its introduction. The material was discovered in the United States, Russia, and Japan in 1941. This material was first seen in reports related to the effect of doping of BaO_2 and TiO_2 on the enhancement of the dielectric properties of piezoelectric ceramics. The dielectric constant of this material is ten times that of other ceramics at that time. In 1945 and 1946, von Hippel, Wul, and Goldman proved the ferroelectric switch in ceramics, which is very important for $BaTiO_3$ ceramics, and proved that ferroelectricity does not always depend on hydrogen bonds but can exist in simple oxide materials. In September 1946, an engineer from the Erie Resistor company realized that the "buzz" was caused by the piezoelectric effect while studying the $BaTiO_3$ capacitor. $BaTiO_3$ is a member of the perovskite family based on the mineral $CaTiO_3$, which can be used in various transducers for mutual electrical and mechanical energy conversion. As a powerful and cost-effective piezoelectric material, Pb (Zr, Ti) O_3 (PZT) has long occupied the piezoelectric ceramic market. In 1954, Jaffe discovered the $PbZrO_3$-$PbTiO_3$ system with high-voltage electrical properties. Doping different elements in Pb (Zr, Ti) O_3 ceramics can change the properties of ferroelectric ceramics. In 1959, L. Egerton and Dolores M. Dillon found that after adding $NaNbO_3$ to $KNbO_3$ in a ratio of 1:1, the resulting $(K_{0.5}Na_{0.5})NbO_3$ has piezoelectricity [27].

$(Bi_{0.5}Na_{0.5})TiO_3$ (BNT) was first reported by Smolenskii et al. in 1960. As an ABO_3 type ferroelectric, the A site is a composite ion of Na^+ and Bi^{3+}. (Bi, Na) TiO_3 ceramics have a high Curie temperature and high polarizability. It is considered one of the options for lead-free ceramics in the future.

Due to environmental problems, the lead contained in PZT materials has attracted widespread attention. In 2006, to protect human health and the environment and exclude or replace harmful substances, the European Union proposed the famous Restriction of Hazardous Substances Directive [28]. The mass fraction of lead oxide in piezoelectric is as high as 60 or more, but so far, piezoelectric devices around the world still lack lead-free alternatives. Researchers have made great efforts to develop multiple lead-free piezoelectric material systems such as (K, Na) NbO_3, $BaTiO_3$, (Bi, Na) TiO_3, and $BiFeO_3$ to explore possible alternatives.

Among all lead-free piezoelectric materials, alkali metal niobate ceramics based on (K, Na) NbO_3 have attracted attention since Saito. The piezoelectric constant of pure (K, Na) NbO_3 ceramics is 80pC/N. After adjusting the texture structure with ions Li-, Ta- and Sb-, the d_{33} of (K, Na) NbO_3 ceramics reached an astonishing 416pC/N in 2004 [29]. Ten years later, through the new phase boundary design of rhombus and tetragonal phase, the d_{33} of (K, Na) NbO_3 ceramics reached 490-570pC/N. Later (2017) the texture-based (K, Na) NbO_3 ceramic obtained a d_{33} of 700pC/N [30].

Compared with other lead-free piezoelectric ceramics, the piezoelectricity of $BaTiO_3$-based ceramics is much higher. In 2009, Ren et al. found that piezoelectric ceramics Ba $(Ti_{0.8}Zr_{0.2})$ O_3-$(Ba_{0.7}Ca_{0.3})$ TiO_3 has extremely high d_{33} (620pC/N) [31]. In 2017, d_{33} 755pC/N and d_{33}* 2027pm/N were realized in (Bi, Ca) (Ti, Zr) O_3 ceramics.

The advantage of (Bi, Na) TiO_3 material lies in the huge strain response. In 2007, the considerable strain value (S=0.45%) of the $Bi_{0.5}Na_{0.5}TiO_3$-$BaTiO_3$-$K_{0.5}Na_{0.5}NbO_3$ ternary ceramic based on the antiferroelectric-ferroelectric phase transition was reported by Zhang *et al.* [32]. In 2016, Tan et al. improved the (Bi, Na) TiO_3 ceramics by using Sr and Nb to obtain a more excellent strain value (S=0.7%) [33]. Since 2003, there have been many reports of substantial residual polarization of $BiFeO_3$ films, but the leakage current caused by impurity phases has affected the quality of $BiFeO_3$ ceramics. In 2015, by improving the production process, $0.67Bi_{1.05}$ $(Fe_{0.97}Ga_{0.03})$ O_3-$0.33BaTiO_3$ ceramics with Rhombohedral-Tetragonal phase boundary obtained d_{33} of 402pC/N and *T*c of 450 degrees Celsius.[34]

2. Lead-Free KNN-Based (KNNS-BZ-BKH)

2.1 Background

2.1.1 Manifestations of piezoelectric properties:

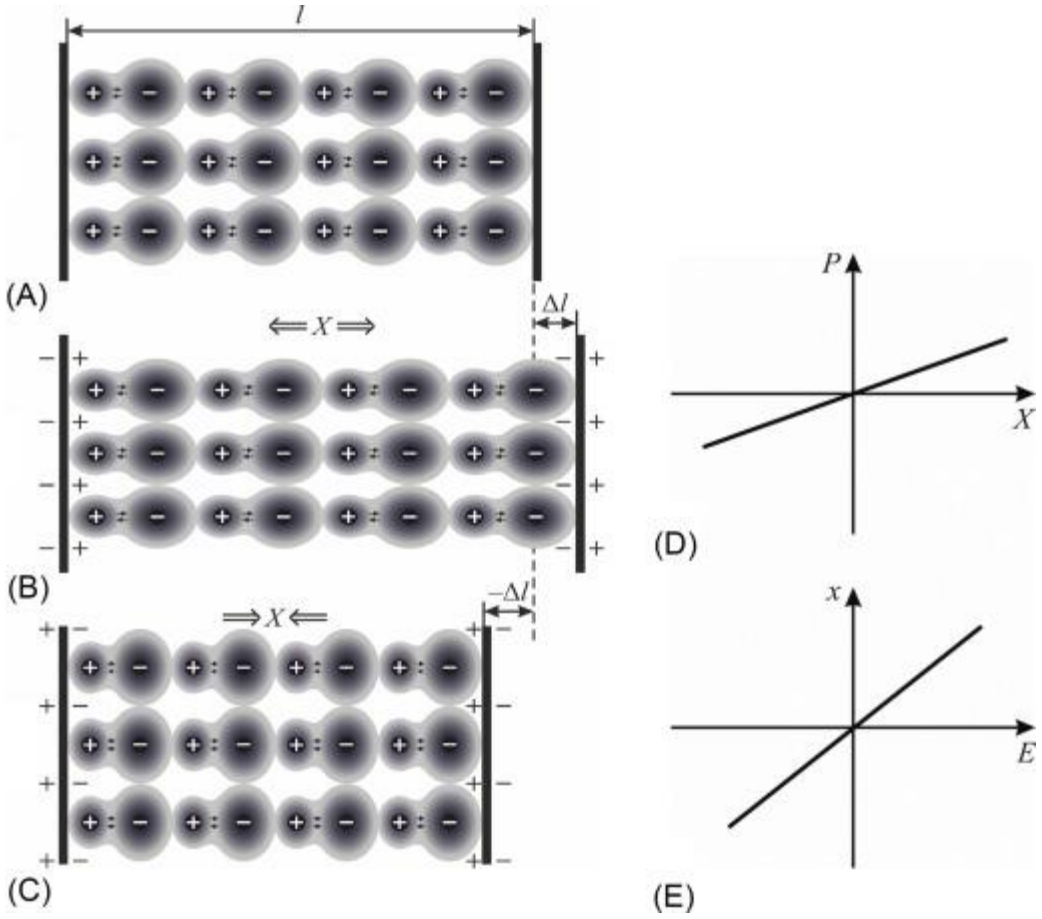

Fig. 6 Longitudinal piezoelectric effect [35]

As shown in Fig. 6, there is a one-dimensional crystal with a length of l, and the internal charges are arranged as (A). After applying tensile mechanical stress to the crystal, the length of the crystal increases by Δ*l*, resulting in an electrical moment (B) with a mechanically induced electric polarization strength of *P*. The relationship between *P* and Δ*l* is shown in (D), and the polarization intensity *P* has a linear relationship with the magnitude of the stress. If compressive mechanical stress is applied to the crystal, the length of the crystal is shortened by Δ*l*, compared to Figure (B), the sign of the compensation charge in Figure C has also changed. Due to the reversibility of the piezoelectric effect, the longitudinal deformation can be obtained by applying an electric field to the crystal; the formula Δ*l*=*d**E, d is the piezoelectric coefficient. Transverse piezoelectric effect:

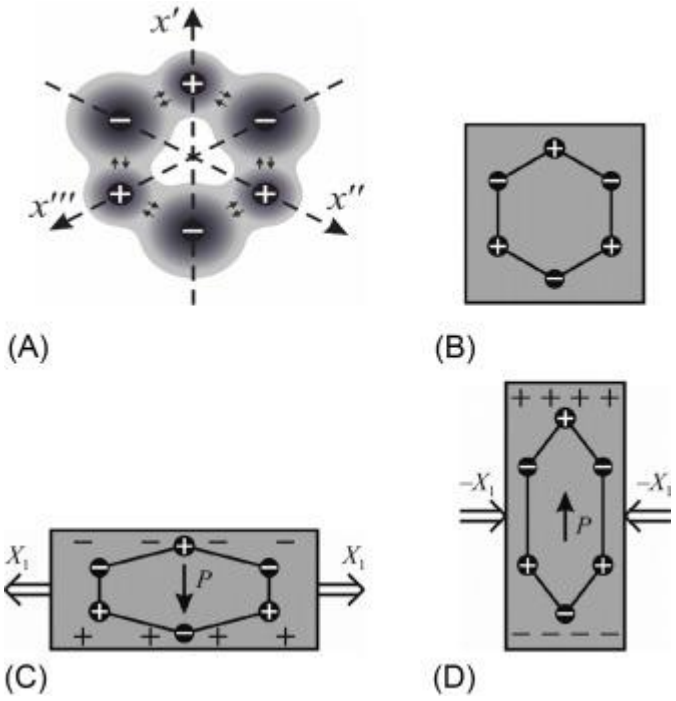

Fig. 7 Transverse piezoelectric effect [35]

The above Fig .7 is a hexagonal α-quartz structure, and the hexagon containing positive and negative ions constitutes a non-centrosymmetric structure (A). Figure (B) shows a two-dimensional square piezoelectric sample that is electrically neutral. After horizontal tensile stress is applied, a transverse piezoelectric effect is produced. The electric polarization is not consistent with the tensile stress direction but is perpendicular to (C). When the stress direction changes, the induced polarity also changes (D). In addition, if mechanical stress is applied along the *x*-axis (A), the longitudinal piezoelectric effect will be observed in this model.

Shear piezoelectric effect:

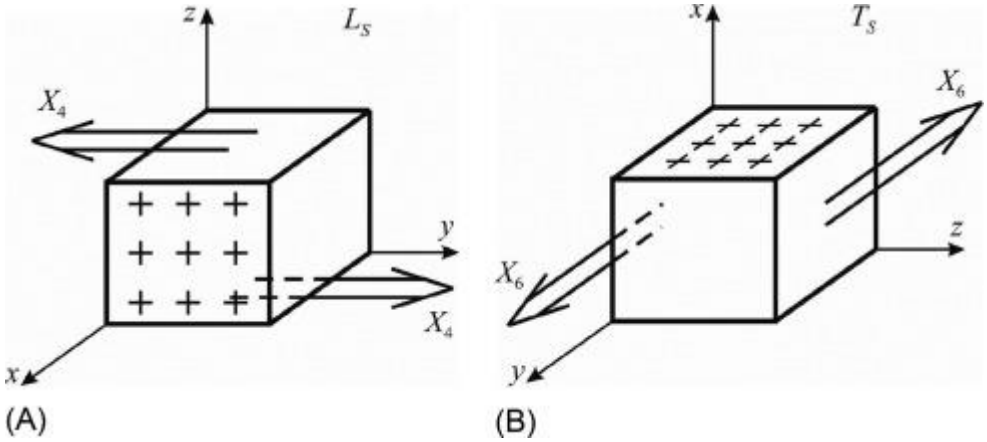

Fig. 8 Shear piezoelectric effect [35]

The three-dimensional crystal model in Fig. 8 has three polar neutral axes: x, y, and z. A mechanical stress perpendicular to the x-axis is applied, and electric polarization along the x-axis is generated inside the crystal.

2.1.2 Piezoelectric and related parameters

Piezoelectricity is a unique property in certain crystalline materials with asymmetric centers. The piezoelectric effect, including the direct piezoelectric effect (electrical polarization after mechanical stress is applied) and inverse piezoelectric effect (mechanical strain after the electric field is applied), is the basis of various electronic devices, such as transducers, actuators, and sensors [36].

2.1.3 The main factors affecting the frequency effect

Generally, the performance of high-voltage electrical materials is as follows: fluctuation structure and domain structure are stable, which affect the influence of conditions.

2.1.4 Phase transition

The phase change of a perovskite material usually affects its ferroelectric/piezoelectric properties. The phase transition point of piezoelectric or ferroelectric materials will vary depending on certain factors (such as composition, temperature, Electric field, or stress); free energy distribution causes phase instability. It is essential to form. Phase boundaries can improve the performance of ferroelectric/piezoelectric materials.

1) Lead-based materials

   Due to its excellent performance, lead-based materials have dominated the past piezoelectric electronic components' application and development. Lead-based piezoelectric materials mainly include ordinary ferroelectrics and relaxor ferroelectrics; the respective representative materials are $(1-x)PbZrO_3$–$xPbTiO_3$ and relaxation-$PbTiO_3$. Currently, The phase boundary design of lead-free piezoelectric materials draws on the concept of the homomorphic phase boundary (MPB) of lead-based piezoelectric ceramic materials [37-41]. A solid solution composed of $PbZrO_3$ and $PbTiO_3$ [$(1-x)PbZrO_3$–$xPbTiO_3$] was first discovered in 1952 by G. Shirane and his colleagues. E. Sawaguchi created the phase diagram in 1953 [42]. In 1954, Bernard Jaffe reported the superior piezoelectricity of the material. Lead-Zirconate-Titanate has a perovskite structure, and Pb induction and MPB endow it with superior piezoelectric properties [43,44]. In addition, the electrical properties of the material can be modified through combination design, "hard"

"Soft" Lead-Zirconate-Titanate can be achieved by doping different components. E.g., Adding low-valent cations (K^+ to replace Pb^{2+}, Fe^{3+} to replace Ti^{4+} or Zr^{4+}) can form oxygen vacancies and limit domain wall movement, reducing piezoelectric performance. Typical representatives of "hard" materials are PZT-4 and PZT-8. High-priced doping can achieve soft Lead-Zirconate-Titanate Cation (La^{3+} replaces Pb^{2+}, Ta^{5+} and Nb^{5+} replace Ti^{4+} or Zr^{4+}), such as PZT-5A and PZT-5H. These designs further expand the usable space of Lead-Zirconate-Titanate materials.

In the past few decades, studies on several typical materials have shown that The coexistence of multiple phases can enhance the properties of ferroelectric and piezoelectric materials. Among them, researchers have studied the perovskite piezoelectric materials in various practical applications, such as transducers, sensors, Actuators, energy harvesting devices, multilayer ceramic capacitors, photovoltaics And electric heating devices, and infrared sensors, etc. Due to the huge d_{33}, $Pb(Zr_xTi_{1-x})O_3$ (PZT) is considered the best piezoelectric material. In this material, the Zr/Ti ratio is modified to achieve a morphotropic phase boundary that is not affected by temperature and ultimately adjusts the electrical properties of the material. The phase structure is susceptible to the nearby Zr/Ti ratio changes. People think that Zr/Ti = 53/ 47. Under morphotropic phase boundary conditions, tetragonal and rhomboid phases coexist in Lead-Zirconate-Titanate. There is a tetragonal phase between the rhombus and the rhombus. However, the theory and experimental methods of morphotropic phase boundary in Lead-Zirconate-Titanate have been questioned by some people. Morphotropic phase boundary is considered to contain mesophase. For example, the synchrotron X-ray powder diffraction measurement method found the monoclinic phase in the $PbZr_{1-x}Ti_xO3$ (x = 0.45–0.5) system. In addition, the most reasonable space group genus of the new monoclinic phase was also observed. In 2001, Noheda and Cox *et al*. It was also found that there are new phases in the phase diagram near morphotropic phase boundary except for the rhomboid phase and the tetragonal phase. In any case, the monoclinic phase existing near morphotropic phase boundary is considered a solid solution $(1 - x)Pb(Zn_{1/3}Nb_{2/3})O_3–xPbTiO_3$ is the cause of the high-voltage electrical coefficient. Given the inconsistency of the melting points of the different components of the solid solution in PZT, it is not easy to manufacture a single crystal PZT. To cope with this problem, a new type of ferroelectric [$A(B1\ B2)O_3$-$PbTiO_3$],

A(B1 B2)O_3 is a relaxor ferroelectric, and $PbTiO_3$ is an ordinary ferroelectric. $Pb(Zn_{1/3}Nb_{2/3})O_3$(PZN) is the main choice for relaxation ferroelectrics, and (1-*x*)$Pb(Zn_{1/3}Nb_{2/3})O_3$-*x*$PbTiO_3$(PZN-*x*PT) single crystals are expected to be high. Based on the early work of Kuwata et al. in 1982, after the development of the manufacturing process, Park and Shrout reported a high-performance relaxed $PbTiO_3$ single crystal in 1990 [45]. In addition, the improved Bridgman method can also be used to obtain large-scale relaxed $PbTiO_3$. The crystal structure of $Pb(Zn_{1/3}Nb_{2/3})O_3$-*x*$PbTiO_3$(PZN-*x*PT) is mainly determined by *x*. PZN and PT are rhombohedral and tetragonal phases, respectively. The large-size PZN-*x*PT single-crystal phase is similar to PZT but has better electrical properties, (*x*=0.28-0.33), d_{33}=1500-2500pC/N, electromechanical coupling factor Kp>0.9. Many studies have tried to uncover the cause of the high-voltage electrical coefficient. Initially, MPB was considered to separate the rhombic and tetragonal phases. However, Cox et al. used X-ray diffraction to detect the MPB of (1-*x*)$Pb(Zn_{1/3}Nb_{2/3})O_3$-*x*$PbTiO_3$ A quadrature-phase was found nearby. Although the actual structure of MPB is in doubt, the function of enhancing piezoelectric performance is undoubted. Since its discovery in 1950, PZT materials have dominated the global piezoelectric materials market. Using MPB design, (1-*x*)Pb(B1 B2)O_3-*x*$PbTiO_3$ can obtain high-voltage electrical performance. However, some application environments require high Tc, such as the automotive and aerospace industries. In order to meet the high voltage electrical performance and high Curie temperature, the material (1-*x*) $BiMeO_3$-*x*$PbTiO_3$ (Me=Sc, In, Yb, Fe) was developed, 0.36$BiScO_3$-0.64$PbTiO_3$ obtained d_{33}=450pC/N, Tc=450 ℃. In the study of PZT materials, inducing the formation of MPB through additives to enhance the electrical performance provides a direction for lead-free piezoelectric materials.

2) Lead-free piezoelectric material

In the study of lead-free piezoelectric materials, it is found that the construction of phase boundaries has a significant effect on enhancing piezoelectric performance. For example, by constructing R-T phase boundaries, d_{33} in $BaTiO_3$ is enhanced (but *T*c is less than 100°C). The phase boundary of most lead-free piezoelectric materials is usually extremely sensitive to temperature and composition. Although MPB can be constructed in $Bi_{0.5}Na_{0.5}TiO_3$, d_{33} and T_d are too low and have minimal application environments. The

research phase boundary construction is of great significance to the research and development of lead-free piezoelectric materials.

Barium Titanate ($BaTiO_3$), first developed as a piezoelectric material by the United States, Japan and Russia, has a high coupling factor, good stability, and simple preparation. Usually, the phase transition temperature of barium titanate is Tc (120℃), T_{O-T}(0℃), T_{R-O} (-90℃). In 2009, the lead-free piezoelectric ceramic $Ba(Ti_{0.8}Zr_{0.2})O_3$-$(Ba_{0.7}Ca_{0.3})TiO_3$ using phase structuring technology obtained d_{33} of up to 620pC/N. Greatly stimulated the research enthusiasm for $BaTiO_3$ piezoelectric materials. Researchers believe that MPB is composed of cubic paraelectric, ferroelectric rhomboid, and tetragonal. D.S.Keeble et al. found an orthogonal phase bridging the tetragonal phase and the rhomboid phase through the X-ray diffraction study of Ba $(Ti_{0.8}Zr_{0.2})O_3$-$(Ba_{0.7}Ca_{0.3})TiO_3$. The tetragonal phase and the rhomboid phase can enhance the piezoelectric performance by deflecting the intermediate phase during the polarization process. Although the $BaTiO_3$ material has the problem of low Curie temperature, which limits the application of the material in terms of temperature stability, the material has played a massive role in exploring lead-free piezoelectric materials.

$BiFeO_3$-based materials have attracted much attention due to their high Curie temperature. In addition to the high leakage current, the lack of MPB seriously hinders the research progress of $BiFeO_3$-based materials in terms of ferroelectric and piezoelectric properties. In BiFeO3-based materials, the composition or strain-enhanced phase boundary for performance enhancement, such as $BiFeO_3/LaAlO_3$ film. Strain driving effectively improves the piezoelectric properties of $BiFeO_3$-based materials. However, ion replacement cannot induce the formation of an effective ferroelectric phase boundary that can improve electrical performance. However, $BiFeO_3$-based materials can enhance piezoelectricity by building phase boundaries with other ABO_3. For example, the solid solution formed by $BiFeO_3$ and $BaTiO_3$ can achieve good piezoelectric performance and high Curie temperature.

(K, Na) NbO_3, because of its relatively good overall performance (K, Na) NbO3 is considered one of the development directions of lead-free piezoelectric materials. Since 416pC/N was obtained on this material by the RTGG method in 2004, researchers have spent much energy constructing the O-T phase boundary based on (K, Na)NbO3 materials.

For example, the 320-324pC/N of Jing-Feng Li group and good temperature stability. Jiagang Wu's R-T phase boundary construction has made a significant breakthrough in d_{33} and confirmed that the high d_{33} value could be attributed to the coexistence of the "nano-scale strain domain" and the construction of the R-T phase boundary. In industrial applications, temperature stability is very important. For a long time, (K, Na)NbO_3 materials have been considered extremely sensitive to ambient temperature. The main research direction is to improve the temperature stability and piezoelectricity of (K, Na)NbO_3 materials through composition modification.

For $Bi_{0.5}Na_{0.5}TiO_3$-based materials, MPB (I) with ferroelectric rhomboid and tetragonal phase boundaries and MPB (II) with ferroelectric and relaxed pseudo-cubic phase boundaries coexisting can be obtained by doping with different additives. Near MPB (I), the peak piezoelectric constant accompanies the saturated P-E curve. The d_{33} from MPB(I) strongly depends on the depolarization temperature (T_d), which severely limits the practical application of this material. The strain enhancement shows that it is related to MPB (II). MPB in BNT not only affects electrical performance but also changes temperature stability.

2.1.5 Microstructure

Both composition and microstructure can affect the physical properties of ferroelectric/piezoelectric materials.

1）Grain morphology

The microstructure of ferroelectric/piezoelectric materials will be affected by the following factors: sintering method, sintering aids, sintering environment, element composition, preparation technology, etc. Different sintering methods can change the microstructure of ceramics. For example, the microstructure of hot-pressed samples is finer. Plasma sintering can achieve high-density sintering at a lower temperature. Adding sintering aids can also optimize the microstructure. Changing the sintering environment can change the microstructure, such as sintering (K, Na)NbO_3 samples in a high-oxygen environment. Adding different ions can also change the microstructure, such as adding Ca2+ ions to (K, Na) NbO3. For most ferroelectric/piezoelectric ceramics, the crystal grain morphology will affect the electrical properties of the material, such as reducing pores and increasing density. Independent of the phase boundary control, the grain size will also affect the piezoelectric performance of the lead-free piezoelectric material.

2）Domain structure and electrical properties

The relevant electrical properties of ferroelectric materials are incredibly dependent on the domain configuration, which is also called domain engineering in ferroelectric applications. Domain engineering is one of the essential technologies to enhance the performance of ferroelectric materials. Through experimental observation and theoretical analysis, the ferroelectric domain structure of piezoelectric ceramics has been widely known [46,47], and domain switching can change the electrical properties of ferroelectric materials. Ferroelectric materials using domain engineering technology have the characteristics of uniform polarization along the direction of the applied electric field. According to previous reports, lead-based materials are prone to 180° and non-180° domain switching near MPB. Different domain types will affect lead-based and lead-free ceramics' electrical activities. In addition to the domain type, the size of the domain also has an important influence on the properties of piezoelectric ceramic materials. Reducing the domain size can significantly increase the piezoelectric coefficient [48-51]. Moreover, the size of the domain is highly related to the phase structure. The coexistence of multiple phases in material increases the complexity of the domain [52]. For example, the monoclinic phase bridging MPB in piezoelectric ceramics can lead to Nano domain structures [53]. Due to the relationship between the phase structure and the polarization process, the domain structure will affect the electrical properties of piezoelectric materials. The microstructure other than the adjustment phase can improve the electrical properties of the piezoelectric material.

3）Polarization

When polycrystalline ceramics are not polarized, the internal domain direction is random. The polarization process is an important step in the piezoelectric ceramic manufacturing process to achieve piezoelectric properties.

In $BiFeO_3$, polarization changes the spontaneous polarization direction, which directly determines the piezoelectric properties [54]. Given the high leakage current and high coercive field characteristics of $BiFeO_3$ ceramics, there are few reports on the polarization research of this material. The non-180° domains of R-phase $BiFeO_3$ ceramics are challenging to deflect due to the force constraints between the crystals [55]. It is worth noting that sufficient electric field strength is required to rotate the polarization domain

direction. If the electric field strength is not enough, extending the polarization time will not help. The polarization temperature is also a critical factor in the polarization process because the domain wall is more active at a high polarization temperature, and it is easier to perform polarization rotation.

For $Bi_{0.5}Na_{0.5}TiO_3$, a DC electric field higher than its coercive field deflects the ferroelectric domains of $Bi_{0.5}Na_{0.5}TiO_3$ ceramics during the polarization process aligns the internal polarization directions. Due to the high coercive field, pure $Bi_{0.5}Na_{0.5}TiO_3$ ceramics are challenging to be polarized. Generally, the polarization process of $Bi_{0.5}Na_{0.5}TiO_3$ based ceramics is optimized by adjusting the chemical composition.

(K, Na)NbO_3.

So far, researchers have invested much energy in optimizing the polarization process of (K, Na)NbO3-based ceramics. (K, Na) NbO3-based ceramics are extremely sensitive to polarization temperature. In general, the optimal polarization temperature of (K, Na) NbO3-based ceramics is at the polycrystalline phase transition temperature. Adding some rare earth materials can reduce the sensitivity of (K, Na) NbO3-based ceramics to polarization temperature [56].

2.2 Production Methods

Most piezoelectric components are made of polycrystalline materials. The piezoelectric ceramics manufacturing process includes powder preparation (material preparation) and sintering of coin samples. The solid-state reaction is widely used in the manufacturing process of piezoelectric ceramics. Before preparing the raw materials, it is necessary to carefully confirm the purity of the material, the shape and size of the particles, and whether the composition is uniform or not.

2.2.1 Powder production

In the powder preparation process, weighing, mixing, drying, and calcination are critical. In general, in order to prepare $(K_xNa_{1-x})NbO_3$ powder, it is necessary to weigh K_2CO_3, Na_2CO_3, and Nb_2O_5, three kinds of raw materials, and then carry out 24 hours of ball milling and 6 hours of calcination (800-900°C), oxide mixing method The disadvantages are large particle size and grinding pollution.

2.2.2 Polyvinyl alcohol

The prepared powder is mixed with polyvinyl alcohol, and the mixed powder is pressed into an appropriate shape using a mold. As a vinyl polymer, polyvinyl alcohol is only connected internally by carbon-carbon bonds. The bond is the same as polyethylene, polypropylene, polystyrene, polyacrylamide, etc. Due to a large number of hydroxyl groups in its molecular chain. Polyvinyl alcohol is water-soluble, biodegradable, has high biocompatibility, and has good mechanical properties and bonding properties. Polyvinyl alcohol can be used to make water-soluble and biodegradable carriers. Applications of polyvinyl alcohol include dyes, washing powders, disinfectants, industrial cleaning chemicals, etc.

Adding polyvinyl alcohol to the material can effectively improve the adhesion, but excessive polyvinyl alcohol will make the sample difficult to shape.

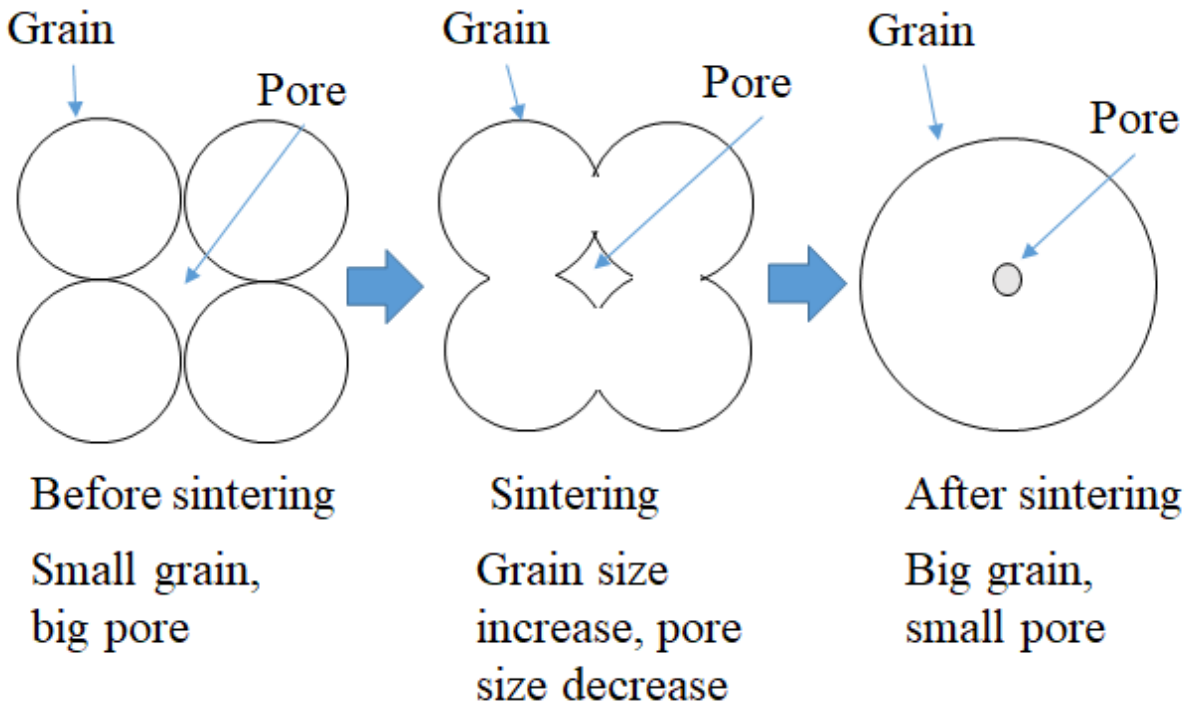

Fig. 9 Mechanism of sintering

2.2.2 Sintering process

The driving force of sintering comes from the minimum energy state caused by the reduction of the total free energy of the object. When the appropriate calcination time and temperature are used, the object reaches the ideal system and reaches its theoretical density; however, if the grain

boundary continues to migrate to reach the single-crystal configuration, the energy state is further reduced. The theoretical density may not be reached in the existing system.

Isolated pores will hinder the sintering process (excessive growth of grains causes the pores not to be eliminated). Over the years, the phenomenon of sintering has aroused widespread interest among researchers. Research on sintering focuses on establishing driving forces, mass transport mechanisms, and the kinetics that lead to particle-particle contact and void elimination processes. On the one hand, researchers study the time and temperature factors that affect sintering to reduce processing costs; on the other hand, they study the microstructure and properties of sintered products to obtain the most suitable materials. At present, it is known that the pretreatment step of sintering is significant. The traditional method is to press the powder and sinter it at an appropriate temperature. The other uses hot pressing to increase the material density, reduce the size of the defects of the material, and reduce the growth of crystal grains. The latest method uses hot pressing to obtain a green body formed by a homogeneous mixture of multiple reactants, and finally, dense composite material is obtained.

Sintering is a synthesis/processing technology in materials and engineering science. It is usually used for metal or ceramic materials and components that use thermal energy to achieve density control.

In recent years, as the importance of material synthesis processing technology has increased, sintering technology has also increased day by day.

The sintering technique, which originated from the firing of prehistoric pottery, is one of the oldest techniques of humanity. However, the scientific community did not research sintering until after the 1940s.

The most extensive use of modern sintering lies in powder metallurgy and ceramic parts. Adjust the internal microstructure of the sintered part by controlling the sintering variables (such as grain size, material density, phase size, distribution, etc.). In most cases, the purpose of microstructure control is to obtain an utterly dense body with a fine-grained structure. During the sintering process, the particles are bonded to form a strong material. Sintering is irreversible because the surface energy between the particles disappears during the sintering process, and bonds are established between the particles. Small particles have higher surface energy and faster sintering speed than large particles.

Because the increase in temperature can promote the movement of atoms, high temperature can accelerate sintering.

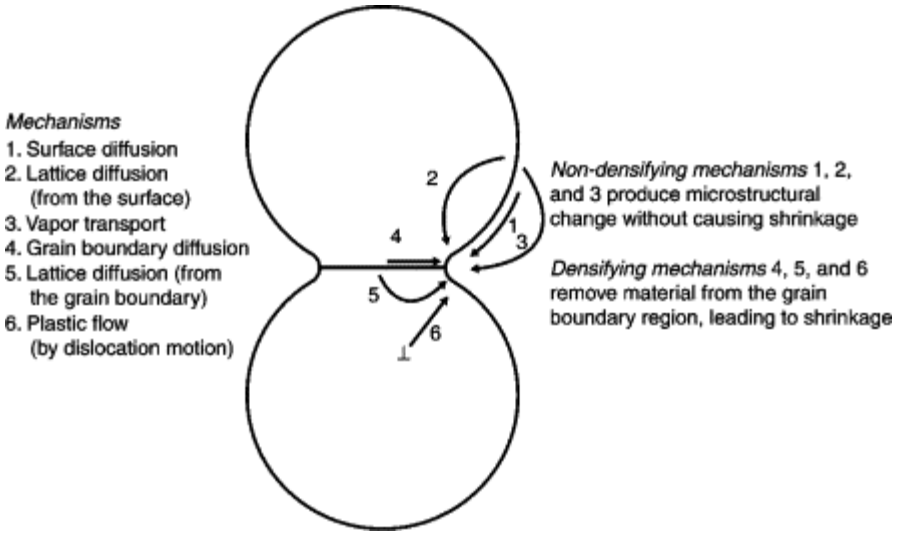

Fig. 10 Process of sintering [57]

As shown in Fig .10 above, the sintering of crystalline materials usually has six ways: surface diffusion, surface lattice diffusion, vapor transmission, grain boundary diffusion, grain boundary lattice diffusion, and plastic flow. Grain boundary diffusion and lattice diffusion are essential factors for the densification of metals and ceramics. The sintering process can generally be divided into three stages: the first stage starts from the neck of the contact particles, in the second stage, the pores between the particles become rounded, and the grains begin to grow, and when the pores are completely closed, the sintering enters the final stage. In one stage, the grains grow further.
The sintering process of the coin sample pressed into a specific shape can effectively increase the density. In general, the sintering temperature is lower than the melting point temperature. The sintering process can eliminate the pores in the sample to significantly increase the sample's density. The factors that significantly impact the sintering process include sintering temperature, sintering aids, sintering atmosphere, and alkali metal loss [58,59]. The optimization of sintering temperature dramatically influences the properties of (K, Na) NbO3-based piezoelectric materials. Different sintering atmospheres will affect the material's microstructure, the phase transition temperature, and then the electrical properties of the ceramic material [60-62].

Sintering methods will also affect the electrical properties of (K, Na) NbO3-based piezoelectric materials. Such as plasma sintering, microwave heating, hot pressing sintering, sealed sintering.

The sintering method that improves the microstructure and suppresses the volatilization of alkali metals can effectively improve the material properties [63-66].

The prominent phenomenon in the sintering process is the solid-state inter diffusion between different compounds, driven by the potential chemical gradient caused by the difference in concentration. The solid-state sintering that occurs in pure powder or alloy powder superimposes the self-diffusion of the material caused by surface and interfacial tension. Fine particle size (small diffusion distance) and high temperature (high diffusion coefficient) are conducive to the sintering reaction.

2.3 Research Work objectives

In this work, we studied the sintering temperature, sintering environment, and K_2CO_3 as an additive to $0.955K_{0.48}Na_{0.52}Nb_{0.9}Sb_{0.1}O_3$-$0.025BaZrO_3$-$0.02Bi_{0.5}K_{0.5}HfO_3$ (abbreviated as KNNS-BZ-BK) ceramic materials the influence of crystallinity and piezoelectric properties.

In addition to the piezoelectric properties of KNNS-BZ-BKH sintered at 850°C and 1210°C, the dependence of crystallinity on the sintering temperature and K^+ additive content is also discussed, and the optimization of the manufacturing process to improve the microscopic morphology and reduction of ceramic materials Defects are formed to increase the dielectric constant of the $0.955K_{0.48}Na_{0.52}Nb_{0.9}Sb_{0.1}O_3$-$0.025BaZrO_3$-$0.02Bi_{0.5}K_{0.5}HfO_3$ material.

3. Experimental Procedure

3.1 Materials Selection

In order to prepare the KNNS-BZ-BKH piezoelectric materials, 99.9% raw reagent-grade of $Bi_{0.5}K_{0.5}HfO_3$, $BaZrO_3$, $K_{0.48}Na_{0.52}Nb_{0.9}Sb_{0.1}O_3$, and K_2CO_3 were used as starting materials. $Bi_{0.5}K_{0.5}HfO_3$, $BaZrO_3$, $K_{0.48}Na_{0.52}Nb_{0.9}Sb_{0.1}O_3$ all have the perovskite structure.

3.1.1 Perovskite

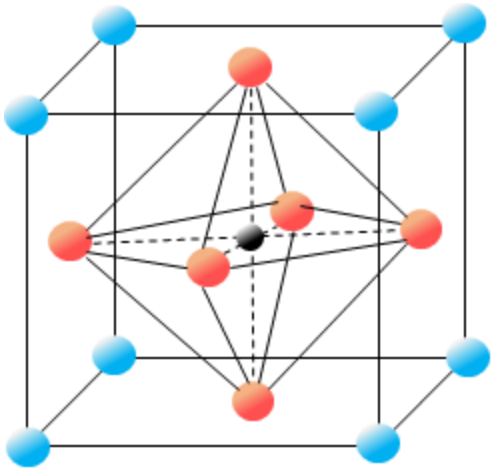

Fig. 11 Perovskite structure

Perovskite is a type of compound with the general formula ABX_3 structure. Its name is derived from the mineral perovskite of the same name. Perovskite is composed of calcium titanium oxide ($CaTiO_3$) and has an orthogonal structure. Many compounds with the general formula ABO_3 have a perovskite structure. Among these compounds, A is divalent, and B is tetravalent. Ca element can be partially or entirely replaced with Na, Mn, Ce, Sr, Pb, and other elements; The Ti element can be replaced with Fe, Nb, Zr, and Mg. Perovskites usually appear as accessory minerals in alkaline and alkaline igneous rocks. Perovskite is commonly found in olivine, yellow feldspar, kimberlite, and carbonate rock with low silica activity. Perovskite is formed during the contact modification of carbonate and usually contains Ce or Nb. $MgSiO_3$ with a perovskite structure is considered the main component of the lower mantle. The perovskite near the earth's surface generally exists in the form of $CaTiO_3$. If the pressure and temperature increase, part of the Ca element will be replaced by Fe, eventually forming $CaFe_3Ti_4O_{12}$. Perovskite is also speculated to be one of the mineral components of the early condensate of the primordial solar nebula.

Perovskite minerals can absorb light. As a semiconductor, the material will generate electric charge movement after being irradiated by light. Methylammonium lead halide is one of the most commonly used perovskite batteries.

Although researchers are still not sure why the light-excited positive and negative charge transfer efficiency in these materials is so high, battery and photovoltaic research has significantly turned to perovskites. Moreover, perovskite reserves are abundant in nature, and the research on

perovskite has also led to the research on superconductivity, magnetoresistance, ionic conductivity, and other characteristics.

The mineral was first discovered in the Ural Mountains of Russia by Gustav Rose in 1839 and was named after the Russian mineralogist L. A. Perovski (1792-1856). In ABX_3, "A" and "B" are two ions, where A and B are cations, A greater than B, and X is an anion. The ideal cubic structure has 6-fold coordination of B cations, surrounded by anion octahedrons, while A cations are in 12-fold cubic octahedron coordination. The ideal perovskite structure is cubic, but Ca, and O are unique to Ti in natural perovskites, which ultimately leads to the orthogonal structure of natural perovskites. With the addition of other elements, the octahedron's degree of inclination and distortion will also change.

The flakes of perovskite are colorless to dark brown and have high transparency. Small-sized crystals may be isotropic, and larger crystals may have weaker birefringence. Nb-, Ce-perovskites are usually dark brown, black, or blue-black.

In the past few decades, inorganic perovskite oxides ($CaTiO_3$, $BaTiO_3$, etc.) and halides have been extensively studied in optical and magnetic fields and are used in electronic products and superconductors. There is also a perovskite material called hybrid organic-inorganic perovskite, which has attracted widespread attention.

Perovskite materials have unique physical properties, such as high absorption coefficient, long-distance bipolar charge transport, low exciton binding energy, high dielectric constant, ferroelectric properties, etc. The application of perovskite materials in photovoltaics and photovoltaics striking. There are different types of perovskite materials in nature, such as chalcogenide perovskite (AMO_3) and halide perovskite (ABX_3), the latter can be divided into alkali metal halides and organometallic halides. Oxyperovskites have excellent ferroelectric and superconducting properties and are widely used. Among the metal halide perovskites, cesium lead halide ($CsPbX_3$) and methylammonium lead halide ($CH_3NH_3PbX_3$) perovskites are the most popular. The halide perovskite structure was discovered in $CsPbX_3$ in 1958. In 1970, researchers started the study of methylammonium perovskite. Methylammonium perovskite has received significant attention due to its excellent optical and electrical properties.

Layered perovskite materials can be applied to thin-film light-emitting diodes (LED) and field-effect transistors (FET). Methylammonium halide (MAX_3) has the characteristics of high absorption coefficient, long diffusion length, and excellent charge transfer characteristics. It is

suitable for photovoltaic applications. Perovskite materials are also widely used in photodetectors, nanolasers, and waveguides.

3.1.2 (K, Na) NbO3

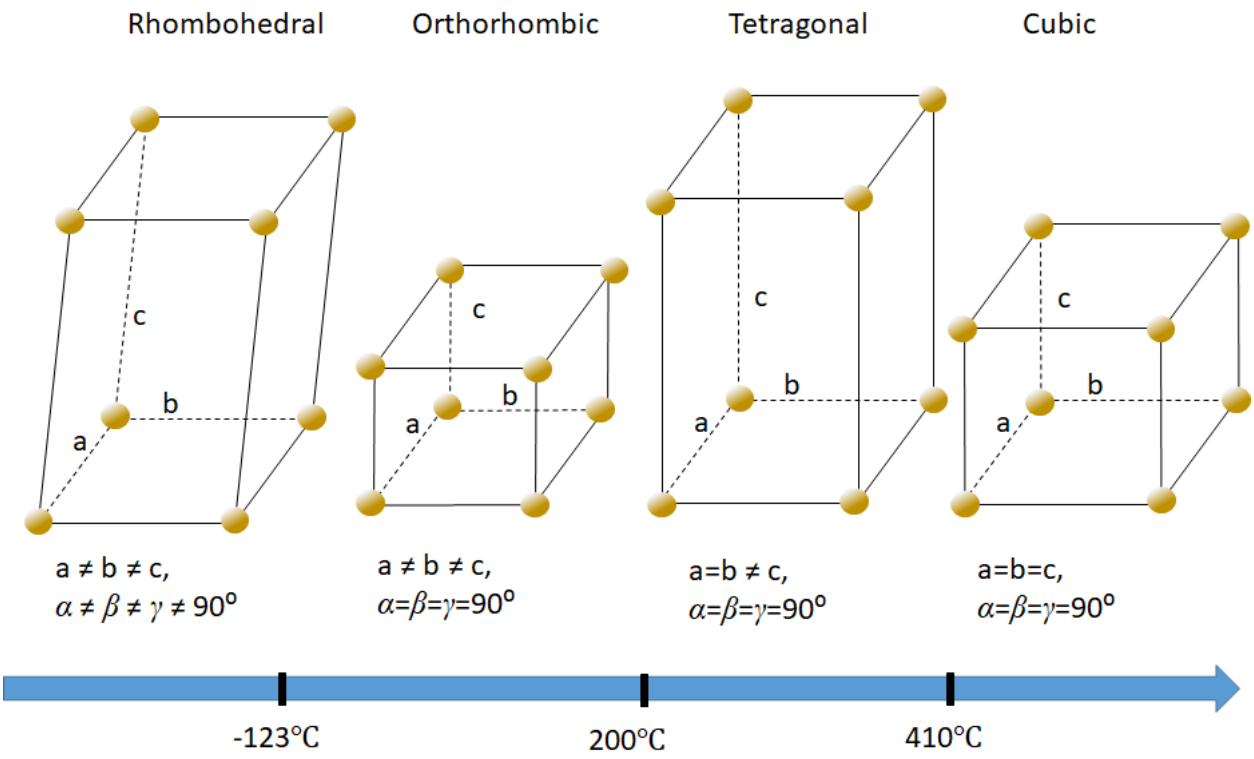

Fig. 12 Phase boundary of (K, Na) NbO_3

Similar to PZT-based piezoelectric ceramics, (K, Na) NbO_3 ceramics are solid binary solutions formed by ferroelectric $KNbO_3$ and antiferroelectric $NaNbO_3$. With temperature changes, (K, Na) NbO_3 ceramics will be at -123℃. It undergoes a trigonal phase→square phase transition, a quadrature-phase→tetragonal phase transition occurs at 210℃, and a tetragonal phase→cubic phase transition occurs at 410℃.

In the preparation of (K, Na) NbO_3 ceramics, the phase transition temperature of (K, Na) NbO_3-based lead-free piezoelectric materials is adjusted to Near room temperature, the material obtains a new phase boundary at room temperature. In the vicinity of the new phase boundary region, there are more possible polarization states because of the coexistence of multiple phases, and the anisotropy between different phases is small. The electrical domains are easily deflected, increasing (K, Na) Properties of lead-free piezoelectric materials based on NbO_3.

By adding a certain amount of Sb^{5+} ions to the (K, Na) NbO_3-based lead-free piezoelectric ceramic material, the ratio of the tetragonal phase in the (K, Na) NbO_3-based lead-free piezoelectric ceramic material can be increased. The orthogonal phase → tetragonal phase The phase transition temperature of the phase is adjusted to near room temperature so that the (K, Na) NbO_3-based lead-free piezoelectric ceramic material transforms from a single orthogonal phase structure at room temperature to the coexistence of orthogonal and tetragonal phases to improve (K, Na) Piezoelectric properties of NbO_3-based lead-free piezoelectric ceramic materials. By constructing a design in which orthogonal and tetragonal phases coexist at room temperature, the piezoelectric performance of (K, Na) NbO_3-based lead-free piezoelectric ceramic materials can be improved it is still larger than Pb(Zr, Ti) O_3 ceramics gap. The addition of Sb^{5+} ions reduces the phase transition temperature of the orthogonal phase→tetragonal phase while adding $Bi_{0.5}K_{0.5}HfO_3$ and $BaZrO_3$ can increase the ratio of the three phases in the (K, Na) NbO_3-based lead-free piezoelectric ceramic material. →The phase transition temperature of the square phase is adjusted from -123°C to around room temperature, and finally, in the room temperature environment, three phases, orthogonal phases, tetragonal phases coexist in the (K, Na) NbO_3-based lead-free piezoelectric ceramic material. There is a new type of phase boundary in which three and four phases coexist. The coexistence of the three-phase, quadrature, and tetragonal phase refers to the simultaneous adjustment of the phase transition temperature of the quadrature-phase→tetragonal phase and the trigonal phase→square phase to around room temperature to achieve three-phase coexistence. The coexistence of the trigonal phase and the tetragonal phase refers to compressing the phase transition temperature region of the orthogonal phase→tetragonal phase and trigonal phase→square phase so that it overlaps near room temperature, and finally in the (K, Na) NbO_3-based lead-free piezoelectric ceramic material Form a new phase boundary. In the multi-phase coexistence state, the energy barrier between phases is low, the polarization reversal is easier, and the electrical properties of (K, Na) NbO_3-based lead-free piezoelectric ceramic materials are optimized.

3.2 Samples Preparation

3.2.1 Powder preparation

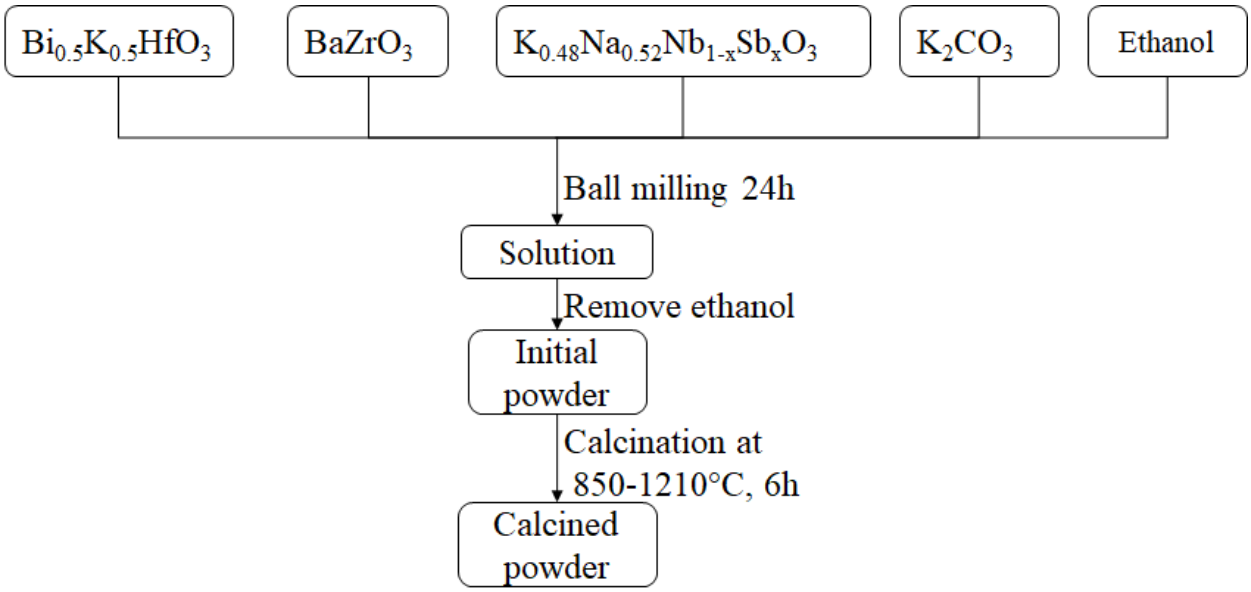

Fig. 13 Powder preparation

To prepare $0.955K_{0.48}Na_{0.52}Nb_{0.9}Sb_{0.1}O_3$-$0.025BaZrO_3$-$0.02Bi_{0.5}K_{0.5}HfO_3$ (KNNS-BZ-BKH) + m K_2CO_3 piezoelectric ceramics, where *m* = 0.0, 0.66, 1.32, 1.98, 2.64, 3.30 And 3.96 mol%, that is approximately *m* = 0, 0.5, 1, 1.5, 2, 3.25 wt%, synthesized by conventional solid-state reaction method, with 99.9% of the original reagent grade $Bi_{0.5}K_{0.5}HfO_3$, $BaZrO_3$, $K_{0.48}Na_{0.52}Nb_{0.9}Sb_{0.1}O_3$ and K_2CO_3 are starting materials.

3.2.2 Conventional solid-state reaction

Fig. 14 Ball milling machine Pulverisette

The solid-state reaction is the most widely used method for preparing polycrystalline solids from a mixture of solid raw materials and is often used to prepare ceramic powders. Solid-state reactions often produce conformal oxides from simple oxides, carbonates, nitrates, hydroxides, oxalates, alkoxides, and other metal salts. The solid-state reaction method can obtain piezoelectric ceramics with thermodynamically stable phases at high temperatures. Before the solid-state reaction, raw material powders such as $Bi_{0.5}K_{0.5}HfO_3$, $BaZrO_3$, $K_{0.48}Na_{0.52}Nb_{0.9}Sb_{0.1}O_3$, and K_2CO_3 need to be mixed with ethanol and ball-milled at 300 rpm for 24 hours (Fig. 14) to ensure the powder's quality Uniform distribution and high contact area. (The initial kinetics of the solid-state reaction largely depends on the contact area between the reacting oxides.) Furthermore, ball milling helps improve the precursor powder's mechanical activity; for example, due to the high impact force in the ball mill, the precursor powder's surface has flat defects, linear defects, or non-equilibrium (Schottky and Frenkel) defects. The ball milling process destroys the initial structure of the precursor powder and increases the surface area of the powder (especially those particles with a size greater than 100 nm). Compared with the powder without ball milling, the self-diffusion coefficient of the powder with enhanced mechanical activation after ball milling is higher. In this way, ball milling accelerates the self-diffusion of the precursor powder, thereby promoting the progress of the solid-state reaction. During the solid phase reaction, in the beginning, $Bi_{0.5}K_{0.5}HfO_3$, $BaZrO_3$, $K_{0.48}Na_{0.52}Nb_{0.9}Sb_{0.1}O_3$, and K_2CO_3 particles contact each other and form $0.955K_{0.48}Na_{0.52}Nb_{0.9}Sb_{0.1}O_3$-$0.025BaZrO_3$ between these particles. -$0.02Bi_{0.5}K_{0.5}HfO_3$ nucleus, the reaction rate after nucleation is affected by the diffusion rate of various ions, and to reduce the size of the electric domain in the piezoelectric ceramic material, it is aimed at a large number of potassium sodium niobate-based piezoelectric materials. This additive reduces the diffusion coefficient. Due to the slow overall kinetics, solid-state synthesis is quite time-consuming. To avoid an incomplete reaction, the precursor powder is exposed to a high temperature for a long time (8 hours in this work). The final product usually consists of thermodynamically stable phases, large and uneven crystallites.

The reaction between solids at room temperature is prolonged. In order to accelerate the reaction rate, the material must be heated to an extremely high temperature to obtain a considerable reaction rate. The factors that affect the feasibility of the reaction and the reaction rate include the chemical and morphological characteristics of the material: the reaction environment, the structure of the reactant, the surface area of the solid, the reactivity between the solids, and the thermodynamic

free energy changes related to the reaction, etc [67,68]. The solid-state reaction is simple to operate and is suitable for large-scale production.

3.2.3 Pellet experiment

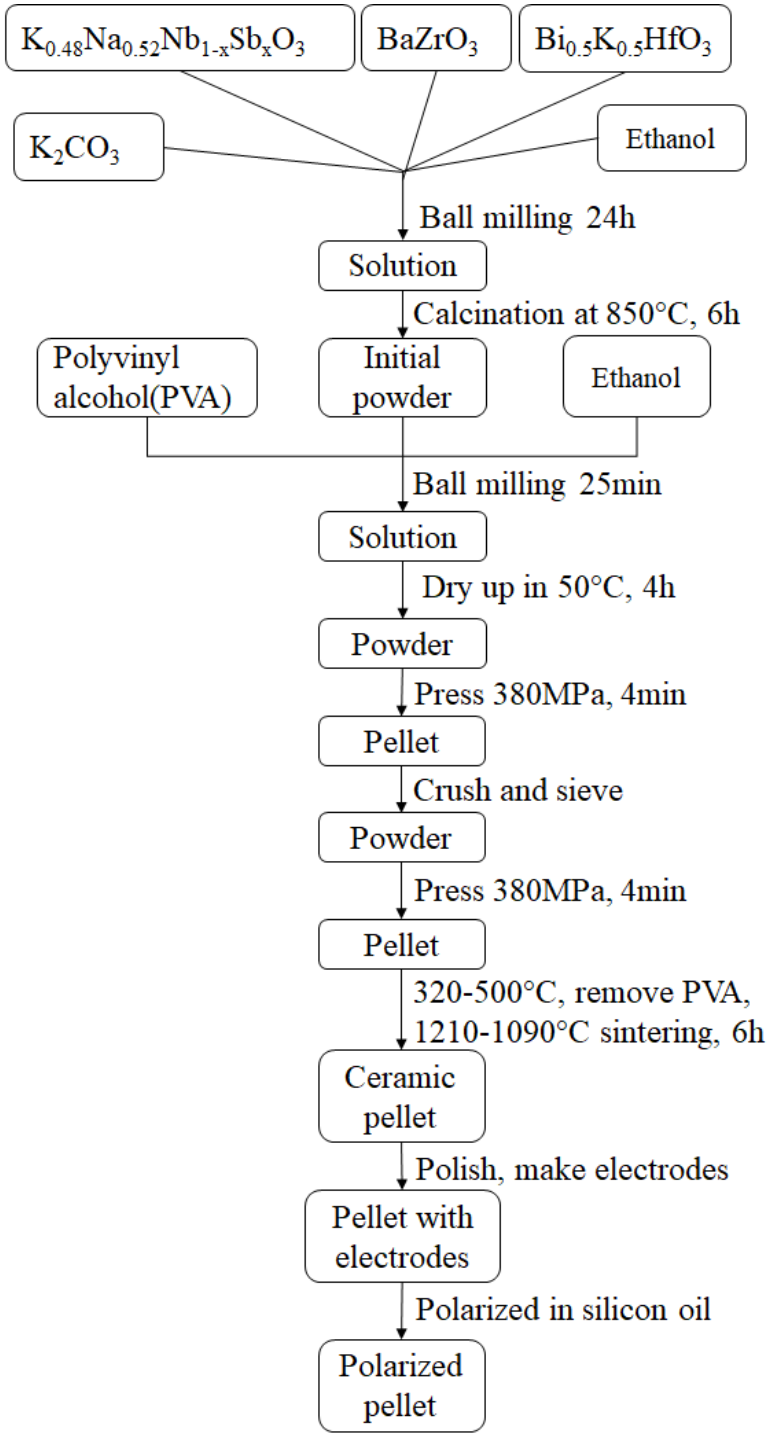

Fig. 15 Pellet sample production

Synthesize (0.955) $K_{0.48}Na_{0.52}Nb_{0.9}Sb_{0.1}O_3$-(0.025) $BaZrO_3$-(0.02) $Bi_{0.5}K_{0.5}HfO_3$ (KNNS-BZ-BKH) + *m* mol% K2CO3 piezoelectric ceramic (*m* = 0.0, 0.66, 1.32, 1.98, 2.64, 3.30 and 3.96 mol%, that is approximately *m* = 0, 0.5, 1, 1.5, 2, 2.5, 3 wt%).

In order to prepare (0.955) $K_{0.48}Na_{0.52}Nb_{0.9}Sb_{0.1}O_3$-(0.025) $BaZrO_3$-(0.02) $Bi_{0.5}K_{0.5}HfO_3$ (KNNS-BZ-BKH) + *m* mol% K_2CO_3 piezoelectric material, with 99.9% of the original reagent Grade $Bi_{0.5}K_{0.5}HfO_3$, $BaZrO_3$, $K_{0.48}Na_{0.52}Nb_{0.9}Sb_{0.1}O_3$ and K_2CO_3 are the starting materials.

First of all, after calculation, weighing, and mixing, the planetary miniature ball mill (Pulverisette) is used for continuous grinding with 7 * 15mm agate balls at 300 rpm for 24 hours (mixed with the appropriate amount of ethanol). Finally, a powder-ethanol solution is obtained. After using a hot plate to heat and evaporate ethanol at 50°C for more than 4 hours, the powder was calcined at 850°C, 1100°C, and 1210°C respectively for 6 hours, and the effect of the calcination temperature on the crystallinity of KNNS-BZ-BKH was compared.

Then, the powder calcined at 850°C is mixed with polyvinyl alcohol (the mass ratio of powder to polyvinyl alcohol is 94:6) and processed into a tablet with a diameter of 10 mm and a thickness of 1 to 2 mm. After burning the PVA, it is sintered at 1090~1210℃ for 6h. Obtain ceramic samples. The silver electrodes on both sides of the sintered sheet are made of silver paint (DuPont, #4922), and polarized in a silicon oil bath of 50-100°C for 10 -120min under a DC electric field of 13~18 kV/cm-1.

Using X-ray diffraction (XRD) and Cu-Kα (λ = 0.15405 nm) radiation source within the angle range of $20° \leq 2\theta \leq 90°$, the calcination of different temperatures and different K additives was characterized at a scan rate of 10°/min The structural properties of the powder. Determine the full width at half maximum (FWHM) of XRD by Voigt function fitting. Energy spectrometer (EDS, HORIBA Scientific) analyzer and scanning electron microscope (SEM, Hitachi SU8010) are used to analyze the microstructure and composition of the sample. In order to overcome the significant error of the EDS peak on the light elements, oxygen was excluded from the estimation to eliminate the influence on the elemental composition analysis. The piezoelectric constant (d_{33}) tester (YE2730A, SINOCERA PIEZOTRONICS INC.) was used to measure the piezoelectric characteristics of the sample.

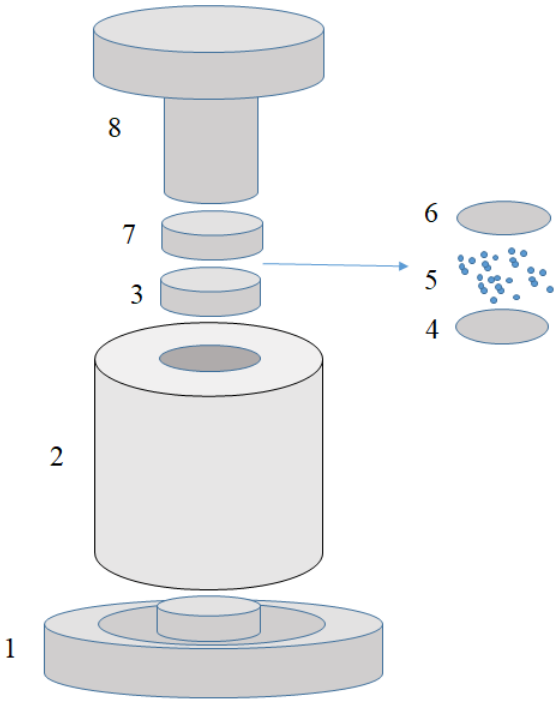

Fig. 16 Pellet press

3.2.3.1 Pellet press

As shown in Fig. 16, it is necessary to use a hydraulic press and a mold to press to obtain a sheet sample. 1, 2, 3, 7, and 8 are all molds.

1) Place mold 2 on base 1;

2) Put in the lower end 3, the diameter is 10mm;

3) Put in puffin paper (diameter 10mm); this is to prevent the sheet sample from sticking to the mold and causing damage to the sample;

4) After ball milling and drying, (0.955) $K_{0.48}Na_{0.52}Nb_{0.9}Sb_{0.1}O_3$-(0.025) $BaZrO_3$-(0.02) $Bi_{0.5}K_{0.5}HfO_3$ (KNNS-BZ-BKH) + *m* mol% K_2CO_3 and poly Vinyl alcohol mixed powder 5;

5) Put another layer of puffin paper (10mm in diameter); the function is also to prevent the sheet sample from sticking and causing damage;

6) Put in the upper end 7;

7) Use the supporting object 8, turn the mold upside down, adjust the position of the lower end 3 (showing half of it is appropriate), and slowly rotate 3. This step is to make the powder distribution in the mold more uniform. If this step is not performed, it may result in a sample. After being suppressed, one side is high, and the other is low;

8) Put in the upper end 9 of the mold, and place the base 1

9) Turn the mold over, take out the upper end 9 of the mold, use the supporting object again, turn the mold upside down, adjust the upper end 7 (exposing half of it is appropriate), slowly rotate 7; this step is the same as step 7), can make the powder inside the mold more uniform;

10) Put in the upper end 9 of the mold, and place the base 1;

11) Adjust the pressure to 30kN and press for 4 minutes to obtain samples.

3.2.3.2 Powder uniform

From the pressed sample to the final ceramic sample, it is necessary to go through the stages of removal of polyvinyl alcohol → sintering → , adding silver electrode → polarization. Among them, the sintering process has a significant influence on the final performance of the sample. In this study, a mesh was used to screen the powder. First, the tableting process is used to keep the internal stress of the powder consistent. After sieving, the powder with the same shape undergoes a compression process to obtain coin samples with a diameter of 10 mm and a thickness of about 1-2 mm.

3.2.3.3 Polyvinyl alcohol removal

Before the sintering process, it is necessary to heat to remove the PVA in the coin sample. In this study, the PVA was removed by heating at 320°C for 4 hours, and then at 500°C for 1 and a half hours to remove the PVA completely.

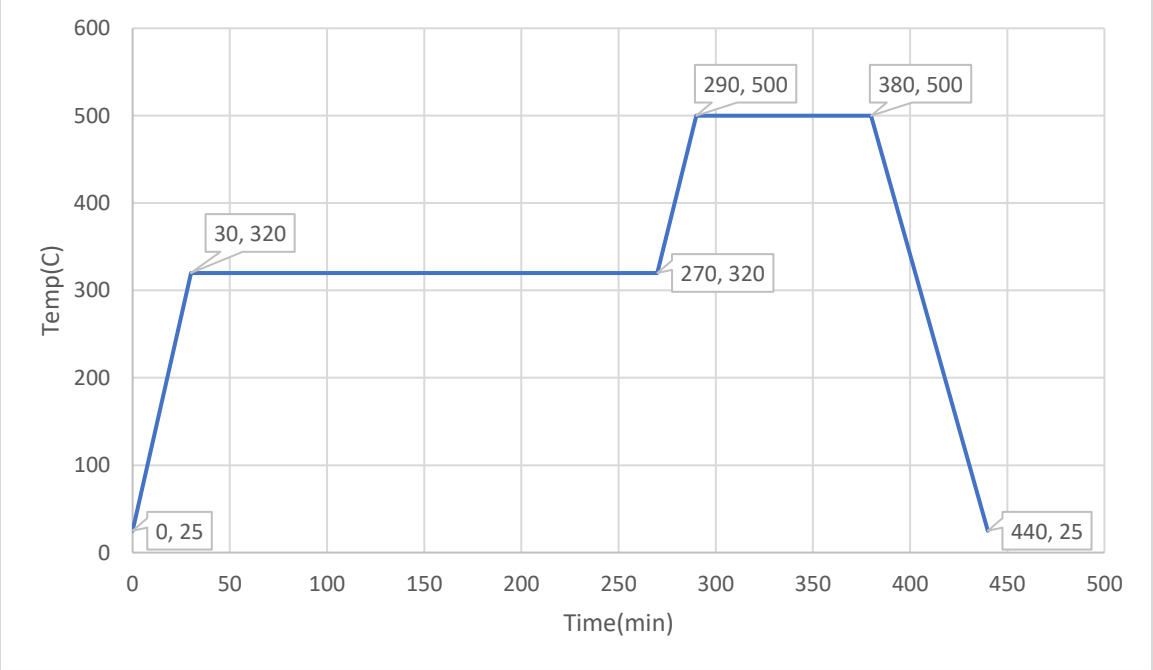

Fig. 17 Polyvinyl alcohol removal heating pattern

Figure 17 illustrates the heating pattern to remove polyvinyl alcohol: When the temperature in the furnace increases to 320°C, polyvinyl alcohol begins to decompose.

Continue for 4 hours to ensure that the polyvinyl alcohol can volatilize slowly and avoid the pores in the pellet sample from being damaged by the volatilization process too fast.

After heating at 320°C for 4 hours, most of the polyvinyl alcohol in the sample has been volatilized. Increase the furnace temperature to 500°C and keep it for 1.5 hours. Under this environment, the polyvinyl alcohol in the sample is removed.

3.2.3.4 Sintering

The sintering process of (K, Na) NbO_3-based ceramic piezoelectric materials has two difficulties:

1) Lighter elements are easy to decompose during the sintering process

2) The sintering temperature of (K, Na) NbO_3-based ceramic piezoelectric materials is susceptible

Fig. 18 Cap sealed by Al_2O_3-water solution

As shown in Fig. 18, given the problem that the lighter elements Na and K in (K, Na) NbO_3-based ceramic piezoelectric materials are easy to decompose, the Al_2O_3-water solution was used in the experiment to create a sealed environment.

In Fig. 18, an Al_2O_3 board and cover are used. First, put an appropriate amount of (0.955) $K_{0.48}Na_{0.52}Nb_{0.9}Sb_{0.1}O_3$-(0.025) $BaZrO_3$-(0.02) $Bi_{0.5}K_{0.5}HfO_3$ (KNNS-BZ- BKH) + *m* mol%

K_2CO_3 powder, this is to avoid the pellet sample sticking to the Al_2O_3 plate after the sintering is completed.

Afterward, put the pellet sample with the polyvinyl alcohol removed on the powder while keeping the pellet sample level, and cover with Al_2O_3 cover. Furthermore, use Al_2O_3-pure aqueous solution to seal the connection between the Al_2O_3 plate and the Al_2O_3 cover, and raise the heating plate to 100℃ When the moisture in the Al_2O_3-pure aqueous solution is evaporated to dryness, the Al_2O_3 powder seals the sample inside the Al_2O_3 plate and the Al_2O_3 cover, and then uses the furnace to sinter the sample.

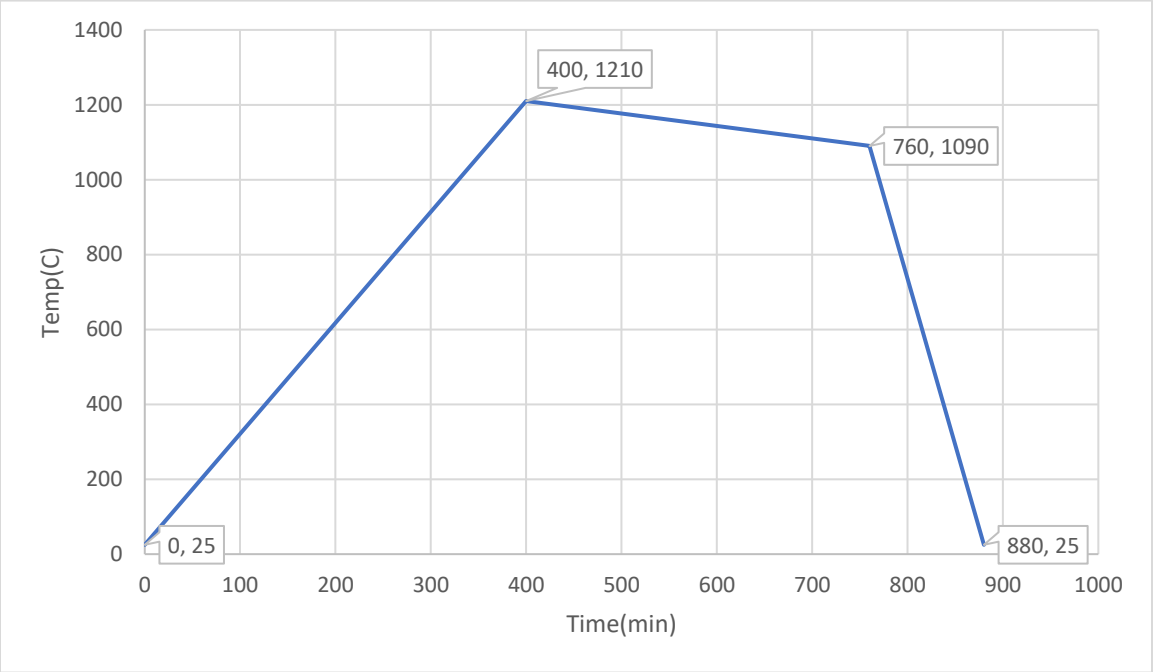

Fig. 19 Sintering pattern

Figure 19 illustrates the heating pattern of the sample sintering. The heating process of up to 6 hours and 40 minutes can avoid the deformation caused by uneven heating inside and outside the sample. (K, Na) NbO_3-based ceramic piezoelectric materials are susceptible to the sintering temperature. If the temperature is too low, the sintering process will not start, and if the temperature is too high, the material will liquefy. After many attempts, this study finally set the sintering temperature to 1210°C. After 6 hours and 40 minutes of slow heating, the temperature in the furnace was slowly reduced to 1090°C over 6 hours. If the furnace is kept at 1210°C for a long time, it will easily cause the sample to liquefy and affect the final performance of the sample. During the 6 hours of slow cooling, the sintering process proceeded slowly, after which the temperature of the furnace was slowly reduced to 25°C. The sintering process of

$K_{0.48}Na_{0.52}Nb_{0.9}Sb_{0.1}O_3$-(0.025) $BaZrO_3$-(0.02) $Bi_{0.5}K_{0.5}HfO_3$ (KNNS-BZ-BKH) + *m* mol% K_2CO_3 is finished.

3.2.3.5 Polarization

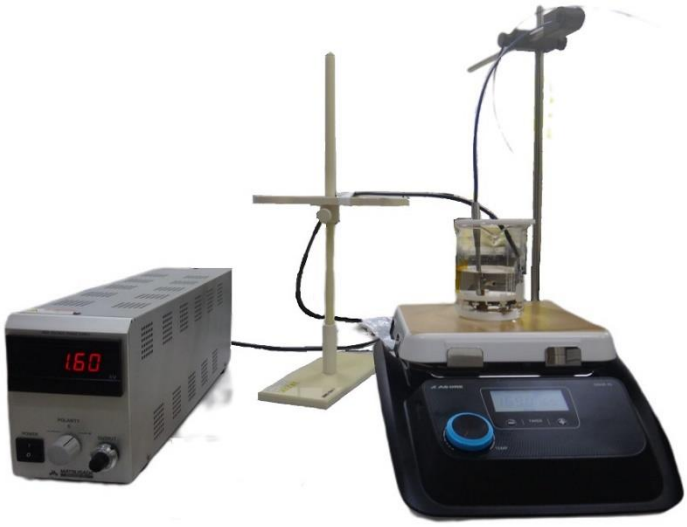

Fig. 20 Polarization device

After coating the two sides of the sintered sample with silver, use the polarization system as shown in Fig. 20 to polarize the sample. The polarization facility consists of a power supply, a heating plate, silicone oil, a bracket, and a fixture. The electric field intensity for polarizing the sample is about 1.6kV/mm, and the temperature of the silicone oil is between 60°C and 100°C.

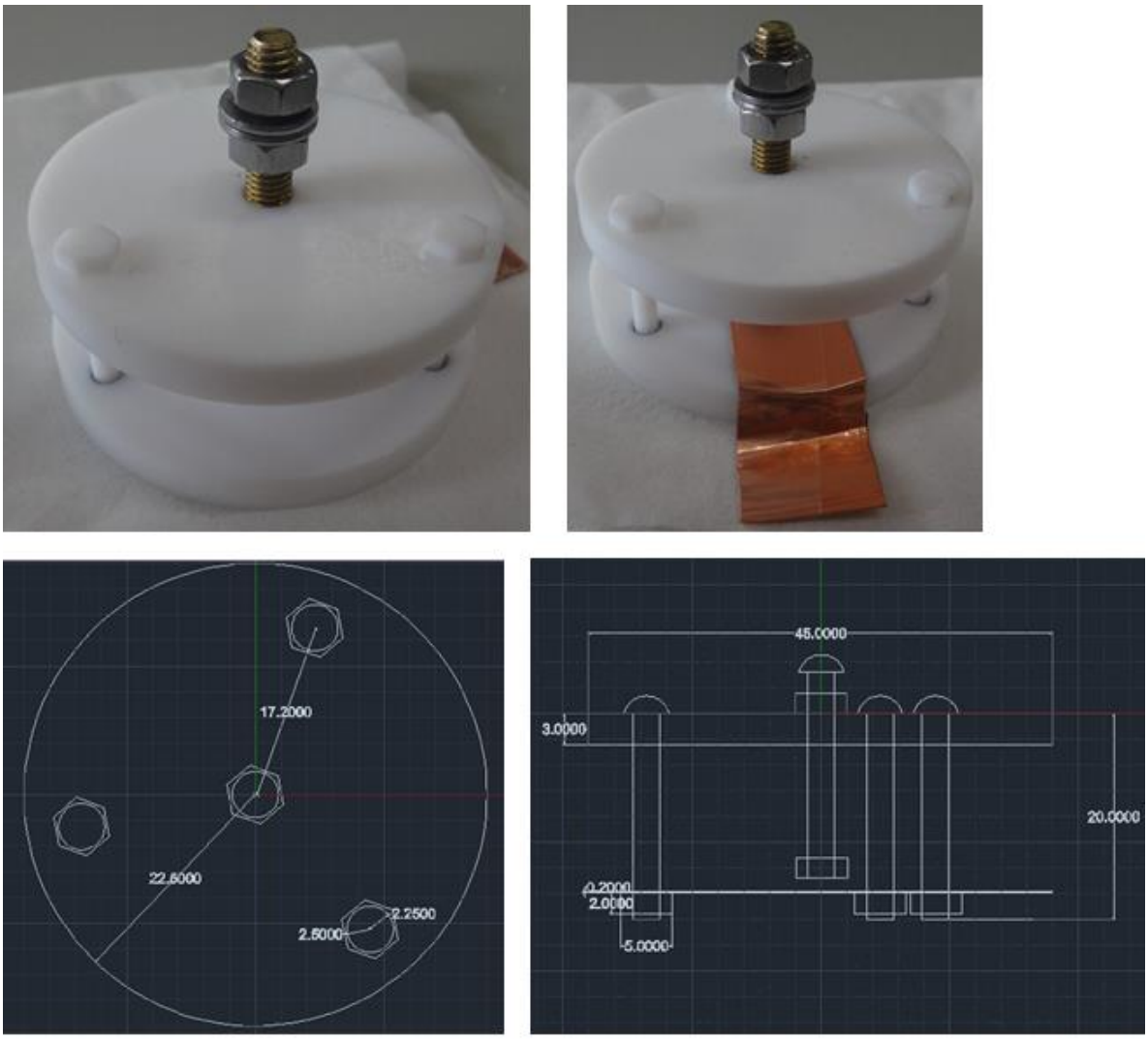

Fig. 21 Sample holder in polarization

Figure 21 shows the fixture, which includes an upper support plate 1, a lower support plate 2, and a support frame composed of an adjustable screw 3. The upper and lower support plates and support frames are all made of polytetrafluoroethylene, and the upper support plate 1 has a through-hole 4 in the center. , The through-hole 4 is provided with a conductive column 5, the conductive column 5 is equipped with an adjusting nut 6, and the conductive column is equipped with a spring 7 between the upper support plate 1 and the adjusting nut 6. Spring 7 can be used to adjust the height. The clamp can be polarized with different thicknesses. Ceramic pieces. A conductive sheet 8 attached to the lower support plate.

The conductive pillar 5 is a copper pillar, and conductive sheet 8 is a copper sheet with good conductivity.

When in use, the height of the conductive column is adjusted according to the thickness of the piezoelectric ceramic sample, the sample is placed between the lower end of the conductive column 5 and the conductive sheet 8, and the piezoelectric ceramic sample is polarized after being energized.

3.3 Analysis Methods

3.3.1 X-ray Diffraction

X-ray diffraction is widely used in research and industry. X-ray diffraction is a type of elastic scattering. X-ray diffraction is especially suitable for the qualitative and quantitative analysis of crystal phases in materials. After in-depth research on X-ray diffraction, more information can be obtained, such as the characterization of solid solution, the size and shape of crystallites, and crystal orientation. X-ray diffraction can be performed at room temperature and normal pressure. Due to its simplicity and ease of use, X-ray diffraction has become the most common method for studying the structural characteristics of nanocomposites.

X-ray diffraction can be used to confirm whether the material is crystalline or amorphous. X-ray diffraction uses an X-ray source of Cu Kα radiation (λ=1.5406 Å) to identify and analyze crystalline compounds by the Brag Brentano method. The Bragg equation is related to the wavelength of the X-ray , the distance between the crystal planes in the crystal, and the angle of incidence.

According to the analysis of the needs of the sample, various parameters such as scanning step length, scanning time, scanning range can be set. The standard database in X-ray diffraction can also be used to compare and identify various crystalline phases.

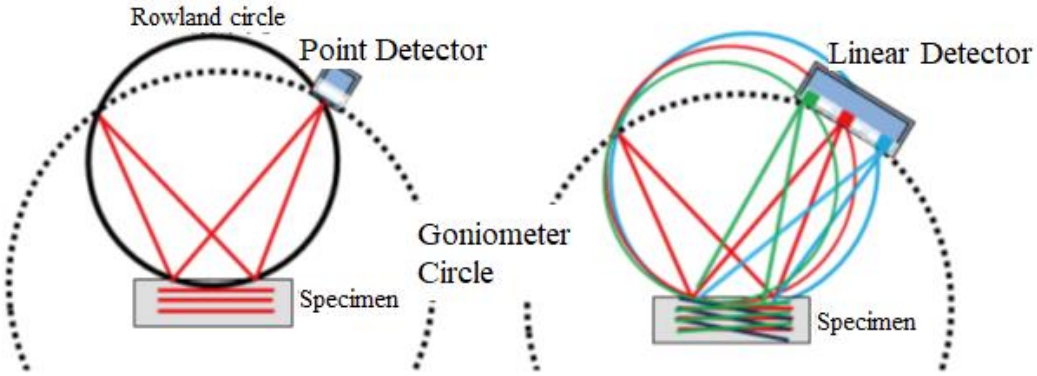

Fig. 22 X-ray diffraction mechanism

As shown in Fig. 22, the X-ray diffraction peaks are produced by the coherent interference of monochromatic X-ray beams scattered at a specific angle from each set of lattice screens in the sample. The position of the atoms in the plane of the lattice determines the peak intensity. From this perspective, the X-ray diffraction pattern can also be seen as a fingerprint of the periodic arrangement of atoms in a given material.

3.3.2 Scanning electron microscope

Scanning electron microscopy technology scans the sample surface through a low-energy electron beam (usually 1 to 30 keV) to create an image of the sample surface with a resolution of up to nanometers. Although the traditional electron microscope is also a high-vacuum instrument, the sample needs to be dehydrated and gold-plated before observation, which can easily cause sample changes. Scanning electron microscopy is widely used to inspect the surface texture of samples qualitatively. The characteristics of a scanning electron microscope are high resolution (10nm), large depth of field. Since the correlation between image brightness and surface height is still unclear, the quantitative analysis of the surface texture of the sample using a scanning electron microscope is not accurate. Scanning electron microscope sample preparation is simple and easy to operate. It is the most important technique for analyzing morphological features such as size and shape.

3.3.3 Energy Dispersive X-ray Spectroscopy

Energy dispersive X-ray spectroscopy can identify elements present in a given material with analysis as an analytical technique used for elemental analysis and chemical characterization of samples. The detection principle of energy-dispersive X-ray spectroscopy is based on: the atomic structure of each element is different, which can form a unique peak group on the X-ray spectrum. In the normal state, the electrons contained in the atoms in the sample are in the ground state or unexcited state. Focusing high-energy charged particle beams (electrons or protons) or X-ray onto the sample, exciting the characteristic X-ray from the sample. The incident light beam excites electrons in the inner shell, and electron holes are generated. After the high-energy electrons in the outer shell release X-ray, they replenish the holes in the inner shell. The sample's elemental composition can be determined by measuring the number and energy of X-ray emitted from the sample.

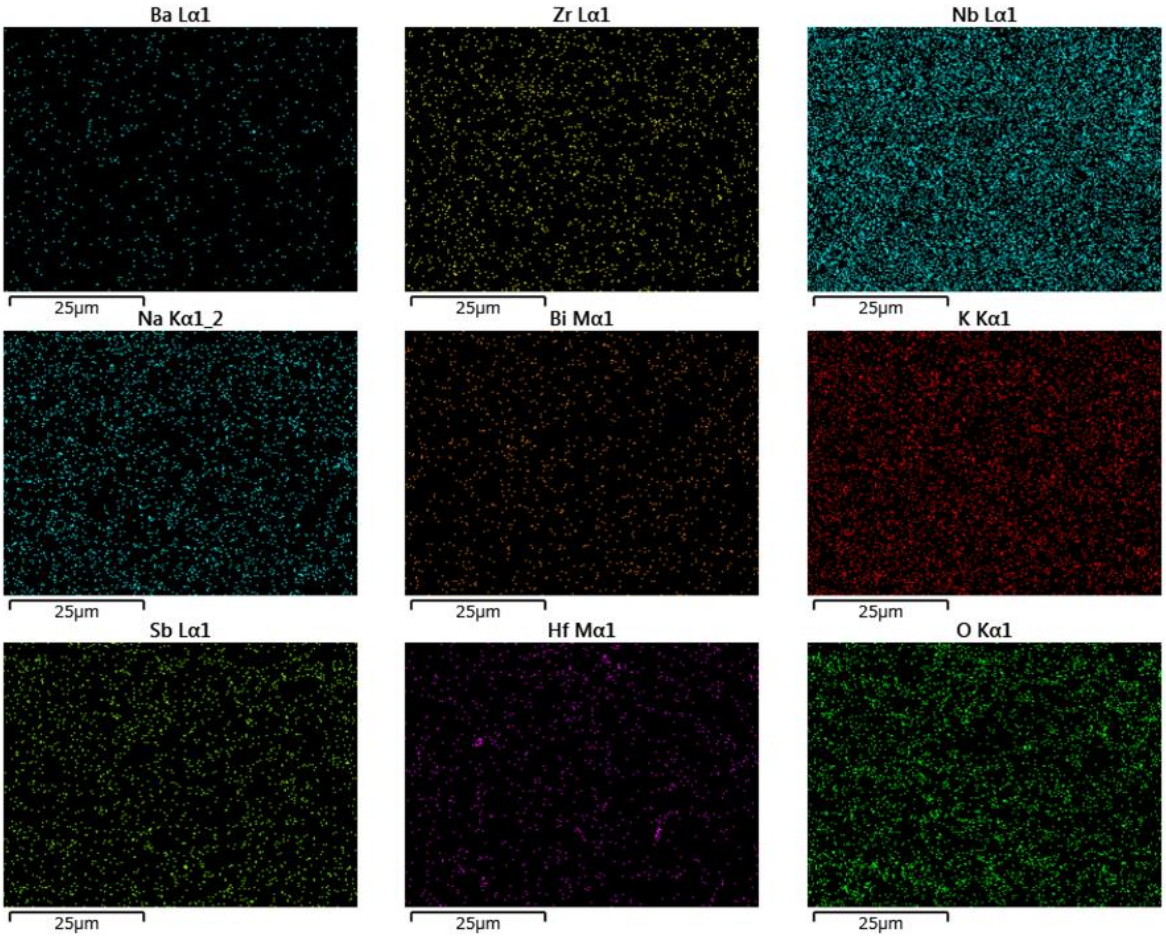

Fig. 23 Energy-dispersive X-ray spectroscopy of different elements

In contrast to energy-dispersive X-ray spectroscopy, wavelength-dispersive X-ray spectroscopy uses diffraction patterns generated by light-matter interactions with finer spectral resolution. However, wavelength dispersive X-ray spectroscopy intelligently analyzes one element at a time, and energy dispersive X-ray spectroscopy can provide a complete spectrum of all elements. Energy dispersive X-ray spectroscopy can be used to identify and quantify the elemental composition of samples with micron size. Energy dispersive X-ray spectroscopy uses energy dispersive detectors to analyze X-rays based on X-ray energy.

4. Results and Discussion

4.1 Structural Evaluation

4.1.1 XRD analysis of powder

The structural properties of the calcined powder with various temperatures and with different K additives were characterized using X-ray diffraction (XRD) with a Cu-Kα (λ = 0.15405 nm) radiation source in the angular range of $20° \leq 2\theta \leq 90°$ and at a scan rate of 10°/min was employed by an X-ray diffractometer (Smartlab, Rigaku Corporation). Full Width at Half Maximum (FWHM) was determined by Voigt function fitting [69].

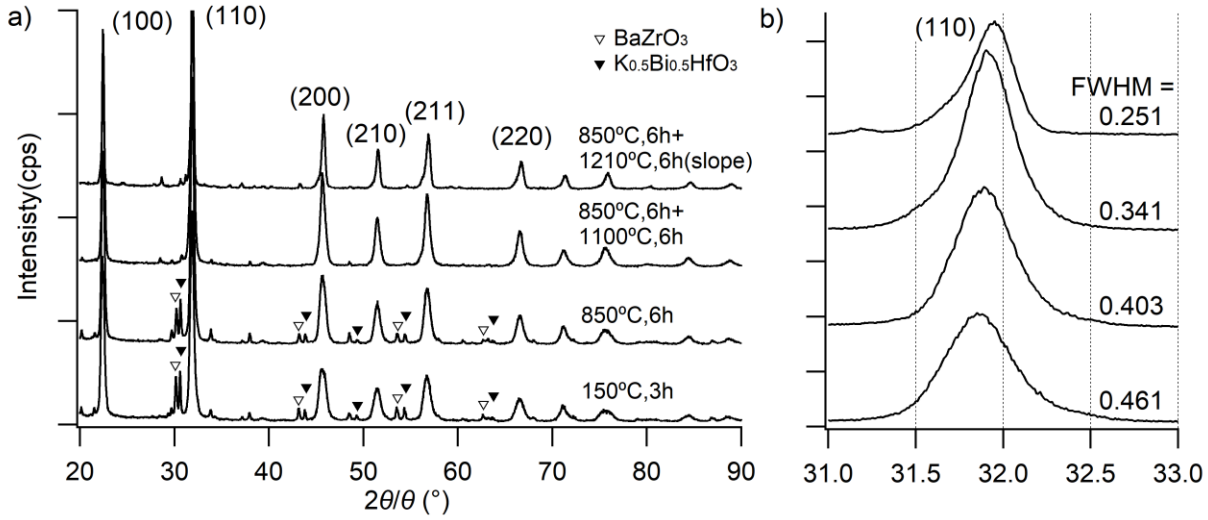

Fig. 24 XRD patterns of powder under different heating patterns (m = 0): (a) the XRD pattern between 20º and 90º; (b) the XRD pattern between 31º and 33º.

Figure 24 (a) shows the powder XRD patterns of the KNNS-BZ-BKH powder prepared without K_2CO_3 additive (*i.e.*, *m* = 0) measured after the following heat treatments: (T1) just after heat treatment at 150℃ for 3h for ethanol removal, (T2) firstly, calcination at 850℃ for 6h, (T3) two-step calcination of firstly at 850℃ for 6h, and secondly at 1100℃ for 6h, and (T4) two-step calcination of firstly with 850℃ for 6h and secondly temperature profile with gradually change from 1210℃ to 1090℃ for 6h. A perovskite structure without a secondary phase was observed for calcined heating patterns of (T3) and (T4). The unreacted raw material peaks as secondary phases in the case of (T1) and (T2) were observed at 2θ=22° (corresponding to KNNS), at 2θ=30°, 43°, and 54° ($BaZrO_3$), at 2θ= 47° and 64° ($Bi_{0.5}K_{0.5}HfO_3$). Fig. 2(b) shows the enlarged peaks of (110) in the 2θ range of 31° to 33°. Broad (110) peaks in only the cases of (T1) and (T2) were observed (FWHM of (T1) = 0.461°, FWHM of (T2) = 0.403°), while sharp (110) peaks in the case of (T3)

and (T4) were observed (FWHM of (T3) = 0.341°, FWHM of (T4) = 0.251°). The (110) peaks moved towards higher angles due to the formation of the KNNS-BZ-BKH perovskite structure. In additional experiments, we found that the secondary heating at a fixed temperature of 1210℃ causes the decomposition of the samples. So, we could conclude that the calcination process with (T4) temperature profile was optimal in the viewpoint of the crystallinity and endorsed the formation of perovskite structure based on the XRD results obtained for KNNS-BZ-BKH powder calcination.

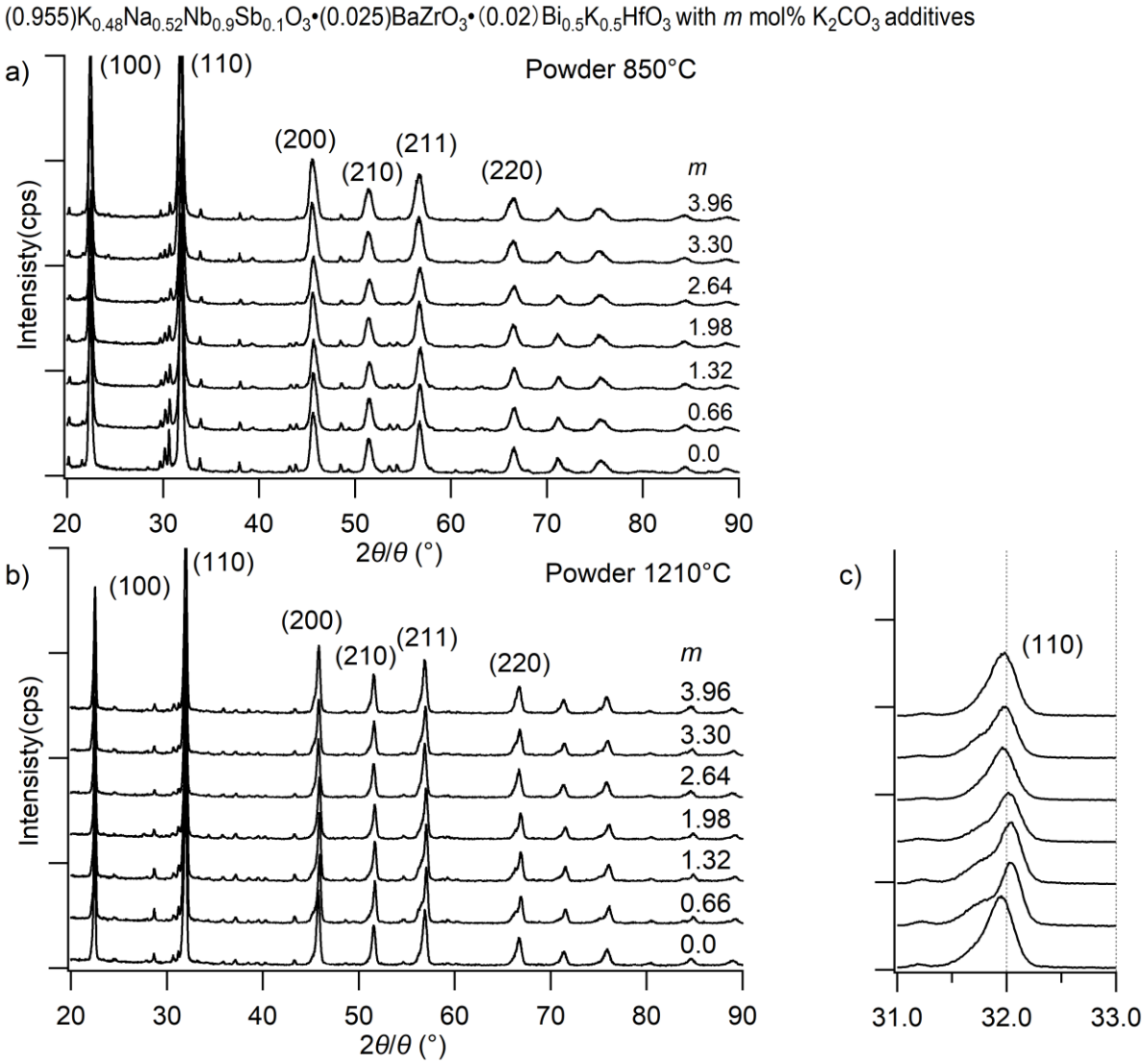

Fig. 25 XRD patterns of powder with different m (a) samples after 850℃ heating (b) (c) samples after 1210℃ heating.

Figure 25 shows XRD diffractions patterns corresponding to KNNS-BZ-BKH ceramics powder doped with different K_2CO_3 amounts (0 to 3.96 mol%) and calcined with (T2) temperature profile (850°C) in Fig 25(a) and (T4) temperature profile (1210°C) in Fig 24(b). A predominant phase related to KNNS with a main orthorhombic perovskite structure has been detected. Small peaks associated with the presence of a secondary phase can be assigned to partially unreacted powder mixture or impurities when calcined under (T2) condition and decrease with an increase in K_2CO_3 additives (*m* mol%). In the case of the calcination under (T4) condition, Fig 25(b) shows a significant decrease in impurity phases even at $m = 0$. In contrast, a more decrease in impurity phases is shown with an increase in *m* led to further suppression of secondary phases. The precise evaluation of the K_2CO_3 *m* mol% additive effect on the crystallinity of KNNS-BZ-BKH ceramics, Fig 25(c) shows an XRD diffraction peak corresponding to (110) at $2\theta = 31.8°$ for KNNS-BZ-BKH powder calcined with (T4) condition. The location of (110) peak increased from $m = 0$ to 1.98 ~ 2.64 mol%, which corresponds to the stoichiometry of K mol% value as shown in Fig 25. While, the increase in the additive *m* over 2.64 mol% led the location of (110) peak to decrease slightly towards lower angles due to excess of K_2CO_3 additives, as shown in Fig 25.

These results showed that K_2CO_3 *m* mol% additive has an optimal range of 1.98 ~ 2.64 mol% in which KNNS-BZ-BKH crystallinity is enhanced via impurity phases removal or entirely reaction of mixture led to the appearance of perovskite structure without secondary phases induced by unreacted raw materials due to highly volatile K element during sintering process with (T4) condition. The diffraction peaks shift toward a higher angle with increasing K_2CO_3 addition since it is expected that K^+ (0.164 nm) could substitute for Bi^{3+} (0.14 nm) and Na^+ (0.139 nm). Only an orthorhombic phase with a perovskite structure was observed. It indicates that the addition of small amounts of K_2CO_3 (0 ~ 3 wt %) did not give rise to an apparent change in the crystal structure.

4.2 Morphology analysis

4.2.1 SEM analysis of powder

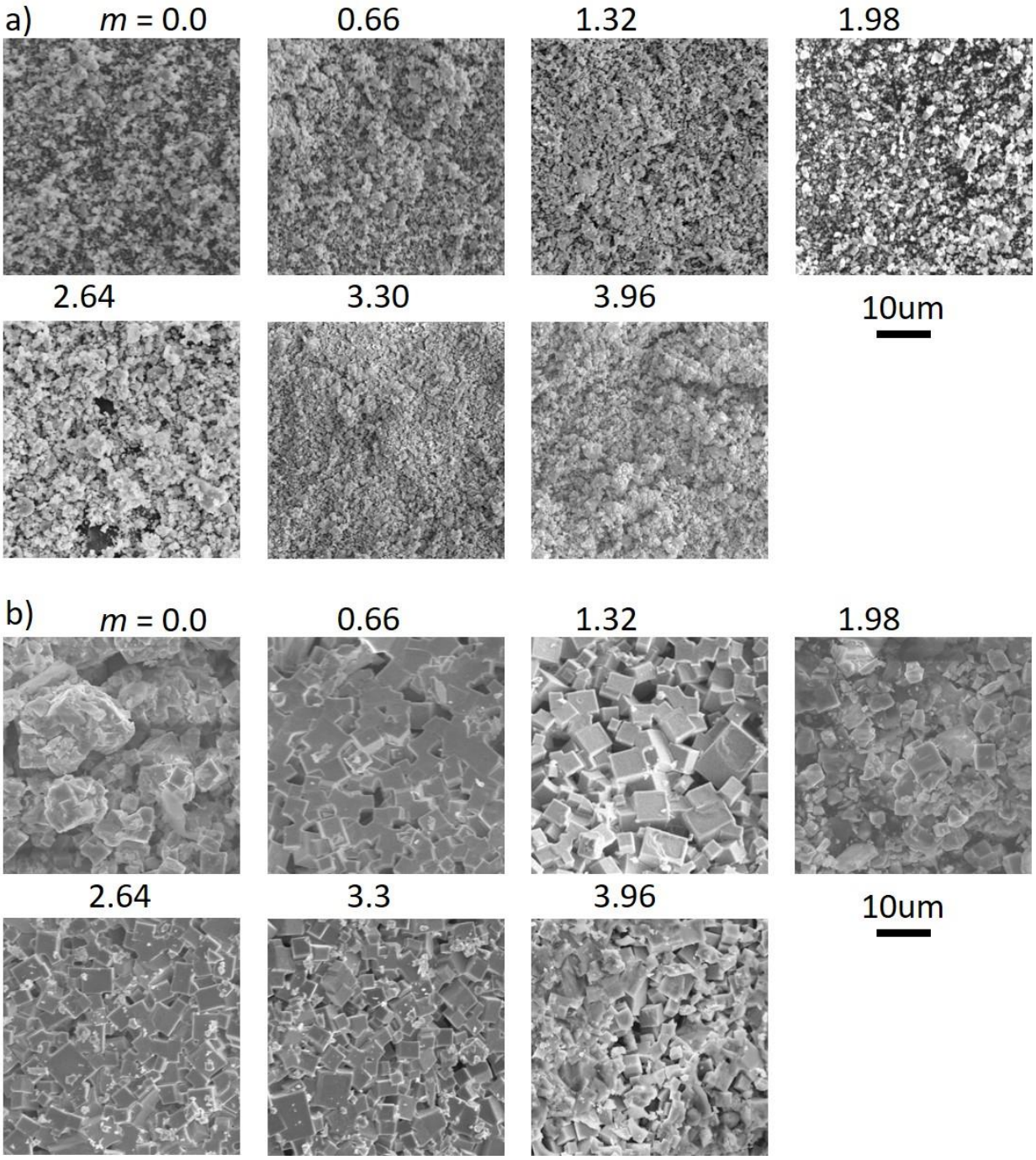

Fig. 26 SEM pictures (2000 magnification) of powder with different m (a) samples after 850℃ heating (b) samples after 1210℃ heating.

Figure 26 shows the SEM images of the KNNS-BZ-BKH with 0 ~ 3.96 mol% K_2CO_3 additives, ceramics sintered with (T2) temperature profile (850℃) in Fig. 5(a) and (T4) temperature profile (1210℃) in Fig. 5(b). The pure KNNS-BZ-BKH ceramic powder sintered with (T2) temperature profile exhibited a small grain size (200 - 300 nm), and no noticeable change in the morphology of the specimen occurred even with various amounts of K_2CO_3 additive. On the other hand, in the case of the (T4) temperature profile, the facets based on the crystal structure were observed. The microstructure in which abnormal grains larger than 700 nm and average grains of 300 to 700 nm coexisted was observed with dense microstructure due to overall grain growth. The most apparent facets were observed at m = 1.32, but the gaps between the grains were rather large. It seems that additives with m = 1.98 to 3.3 show denser morphology, with facets being nucleated. This change in the grain gap may be correlated with the change in the (110) peak shown in Fig 24(c) [69].

4.3 Composition Analysis

4.3.1 XRD analysis of powder

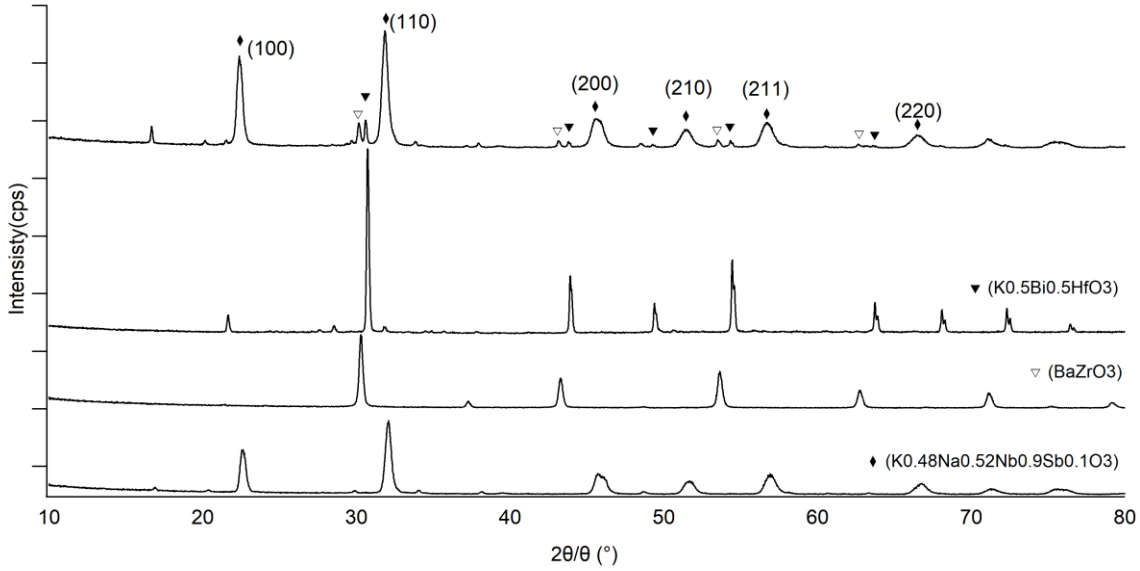

Fig. 27 X-ray diffraction pattern of initial powder and material $0.955K_{0.48}Na_{0.52}Nb_{0.9}Sb_{0.1}O_3$-$0.025BaZrO_3$-$0.02Bi_{0.5}K_{0.5}HfO_3$

The preparation of the sample needs to go through the processes of raw material→piezoelectric material→piezoelectric ceramic sample→polarization. In order to ensure the consistency of the material, we compared the initial powder $Bi_{0.5}K_{0.5}HfO_3$, $BaZrO_3$, $K_{0.48}Na_{0.52}Nb_{0.9}Sb_{0.1}O_3$ with the synthetic material $0.955K_{0.48}Na_{0.52}Nb_{0.9}Sb_{0.1}O_3$-$0.025BaZrO_3$-$0.02Bi_{0.5}K_{0.5}HfO_3$ The X-ray diffraction pattern of (as shown above), it can be seen that the phases of powder $Bi_{0.5}K_{0.5}HfO_3$,

$BaZrO_3$ can be observed at 21-22°, 30°, 45°, 55°, and 65°. After ball milling, The mixed powder heated at 850°C only undergoes basic fusion, and there is still a gap between the final target product.

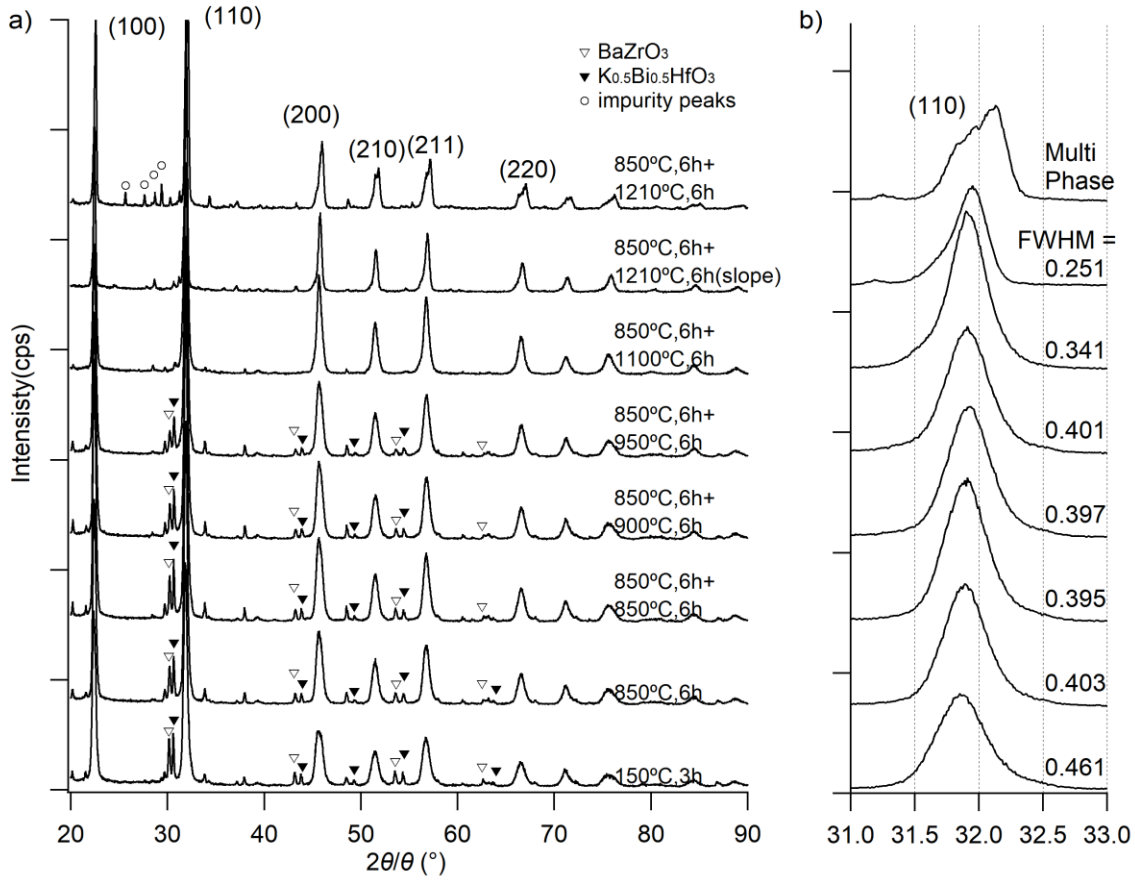

Fig. 28 X-ray diffraction pattern under different temperature of material $0.955K_{0.48}Na_{0.52}Nb_{0.9}Sb_{0.1}O_3$-$0.025BaZrO_3$-$0.02Bi_{0.5}K_{0.5}HfO_3$

In order to further confirm the specific experimental process of raw material→piezoelectric material→piezoelectric ceramic sample, as shown in the figure above, the initial powder $Bi_{0.5}K_{0.5}HfO_3$, $BaZrO_3$, $K_{0.48}Na_{0.52}Nb_{0.9}Sb_{0.1}O_3$. In the process of $0.955K_{0.48}Na_{0.52}Nb_{0.9}Sb_{0.1}O_3$-0.025BaZrO3-0.02Bi0.5K0.5HfO3, we tested:

1) After ball milling the raw materials, heat the mixed powder at 150°C to entirely remove the ethanol and water in the mixed powder, and perform XRD analysis on the powder sample;

2) After ball milling the raw materials, heat the mixed powder at 150°C, and use the furnace to heat the sample powder at 850°C for 6 hours to make the solid-state reaction wholly proceed, and then perform XRD analysis on the powder sample;

3) After ball milling the raw materials, heat the mixed powder at 150°C and 850°C, heat the powder sample at 850°C for 6 hours. This sample is an experimental group designed to compare with other samples that have been heated multiple times. , Perform XRD analysis;

4) After ball milling the raw materials, heat the mixed powder at 150°C and 850°C, then heat the powder sample at 900°C for 6 hours, and gradually increase the heating temperature to observe the XRD image of the comparative powder;

5) After ball milling the raw materials, heat the mixed powder at 150°C and 850°C, then heat the powder sample at 950°C for 6 hours, and gradually increase the heating temperature to observe the XRD image of the comparative powder;

6) After ball milling the raw materials, heat the mixed powder at 150°C and 850°C, then heat the powder sample at 1100°C for 6 hours, and gradually increase the heating temperature to observe the XRD image of the comparative powder sample;

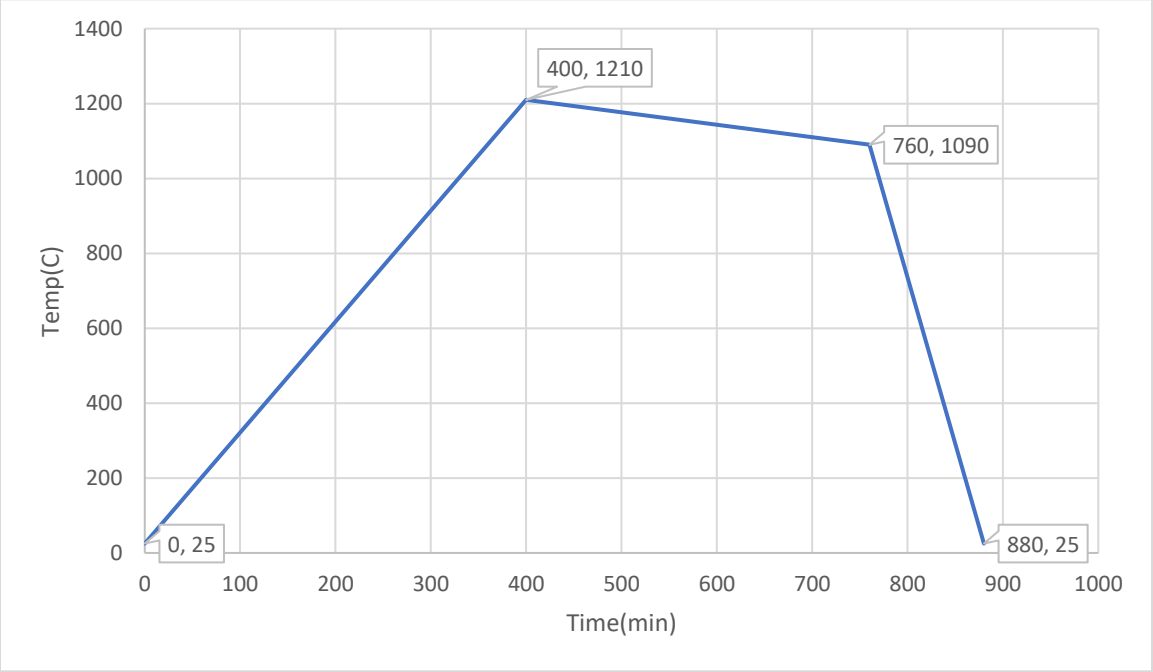

Fig. 29 1210°C heating pattern(slope)

7) After ball milling the raw materials, heat the mixed powder at 150°C and 850°C, then heat the powder sample at 1210°C (slope, the specific heating pattern is shown in the figure above), and observe the XRD image of the comparative powder sample;

8) After ball milling the raw materials, heat the mixed powder at 150°C and 850°C, then heat the powder sample at 1210°C for 6 hours, and gradually increase the heating temperature to observe the XRD image of the comparative powder sample;

Comprehensively comparing the above XRD pattern, we find that:

1) In the heating range from 150°C to 850°C, the XRD pattern of the powder sample does not change much, and the phases belonging to the original powder Bi0.5K0.5HfO_3 and $BaZrO_3$ can be observed (the inverted triangle pattern in Fig. 28);

2) After heating at 850°C or 900°C and 950°C twice, a part of the original powder Bi0.5K0.5HfO3 and $BaZrO_3$ phases begin to disappear (at about 64°). It can be inferred that the temperature range is 900-950°C. The solid-phase reaction between the powders begins;

3) After the temperature rises to 1100℃, the solid phase reaction between the original powders $Bi_{0.5}K_{0.5}HfO_3$, $BaZrO_3$, $K_{0.48}Na_{0.52}Nb_{0.9}Sb_{0.1}O_3$ is relatively complete, forming a relatively single orthogonal phase, and the crystal orientation 110 gets significantly higher crest;

4) After heating at 1210°C (slope), it can be observed that the wave peaks at the crystal orientation 110 have a certain degree of separation. At this time, it is speculated that the sample powder has formed a mixture of orthogonal and trigonal phases;

5) After continuous heating at 1210℃, the degree of wave peak separation at 110 crystal orientation is further increased, and the actual heating has exceeded the melting point of the powder. At this time, the piezoelectric performance of the obtained sample is reduced and is no longer suitable for piezoelectric ceramic preparation.

4.3.2 EDS analysis of powder

A scanning electron microscope (SEM, Hitachi SU8010) equipped with an energy dispersive spectrometer (EDS, HORIBA Scientific) analyzer was used for microstructure and composition analysis.

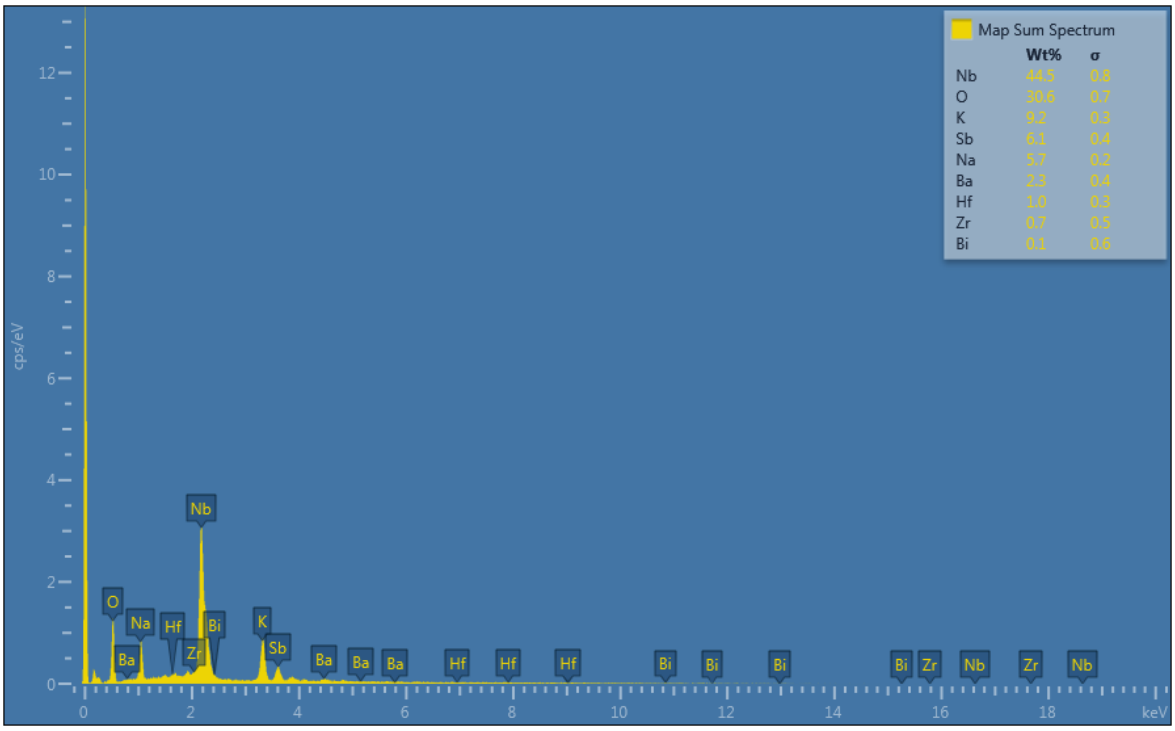

Fig. 30 element analysis report of EDS

The above picture is an element analysis report of a point in a powder sample using the EDS mode. The upper right corner of the picture shows each element's mass score and error range. To ensure data consistency, the EDS data is taken with an error within 1.0. However, considering that a single EDS test only takes data from a specific area, the uniformity of powder distribution in different areas may be different. In the actual data collection, at least 7 areas in the same powder sample are selected for EDS detection, and then the 7 sets of data are averaged. In the actual detection, there is a detection of the mass fraction of oxygen element, but considering the air and moisture and other reasons, the actual data calculation needs to exclude the oxygen element and then perform the calculation.

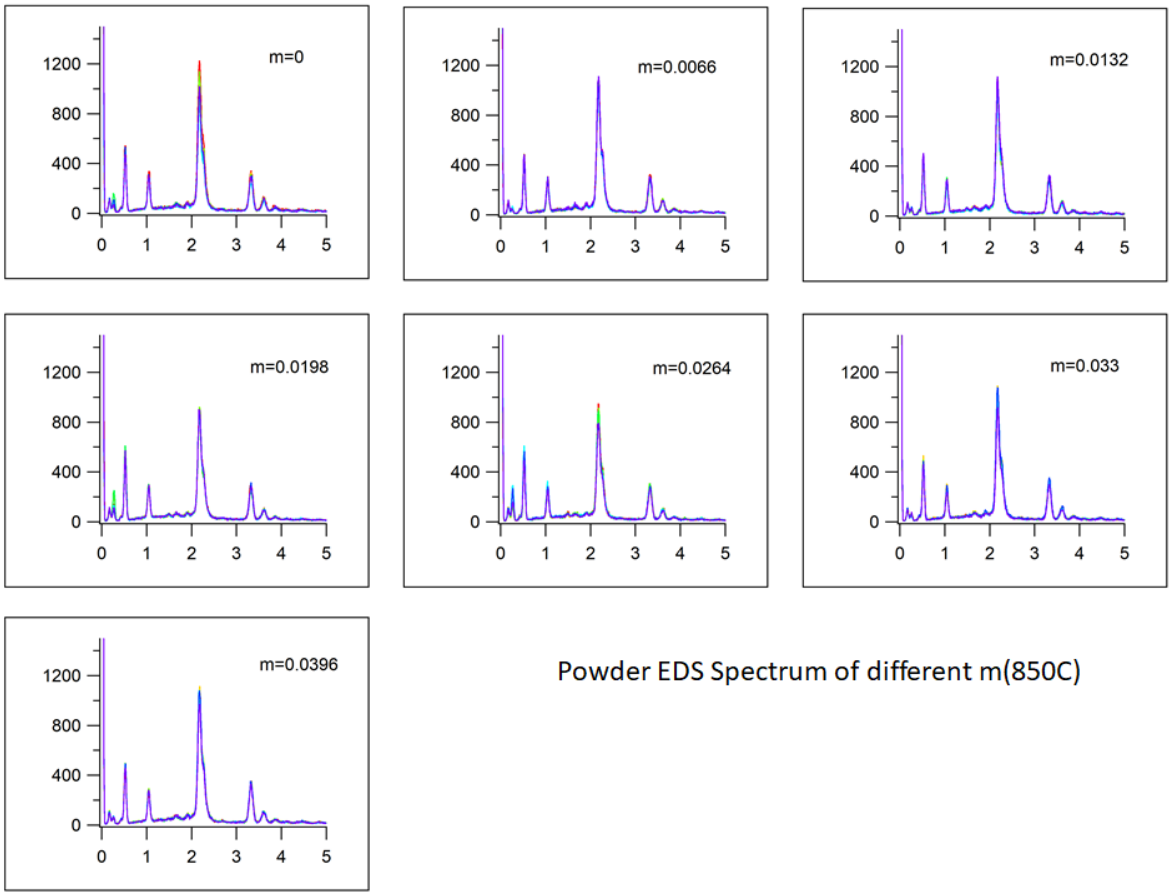

Fig. 31 Powder EDS spectrum under 850°C

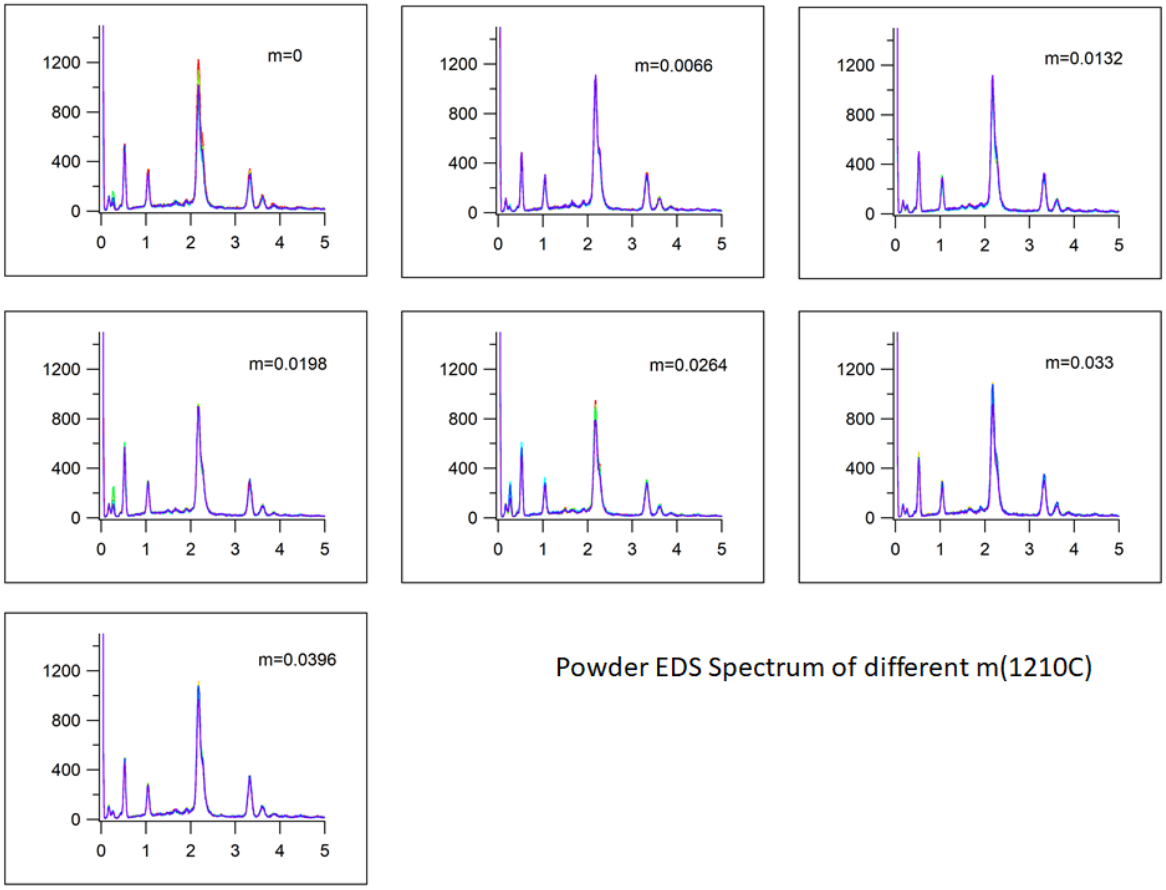

Fig. 32 Powder EDS spectrum under 1210°C(slope)

Before using EDS for testing, the powder needs to be prepared. The state of the powder sample will affect the testing effect of EDS. In order to improve the accuracy of EDS detection, on the one hand, it is necessary to reduce the particle size of the powder sample to ensure that the powder sample is evenly spread on the testing table. On the other hand, it is necessary to dry the powder sample in advance to avoid the adverse effect of moisture on EDS detection.

Figure 32 shows $0.955K_{0.48}Na_{0.52}Nb_{0.9}Sb_{0.1}O_3$-$0.025BaZrO_3$-$0.02Bi_{0.5}K_{0.5}HfO_3$ with additive m K_2CO_3 (m takes 0.0, 0.0066, 0.0132, 0.0198, 0.0264, 0.033, 0.0396 in different situations). After heating at 850°C and heating at 1210°C (slope), each group takes 7 different points for EDS detection (15keV data). After comparison, we found that the scanning results at different points are similar after the powder is ground to reduce the particle size and dried. Generally, the EDS results can be considered credible and used for the elemental composition analysis of powder samples.

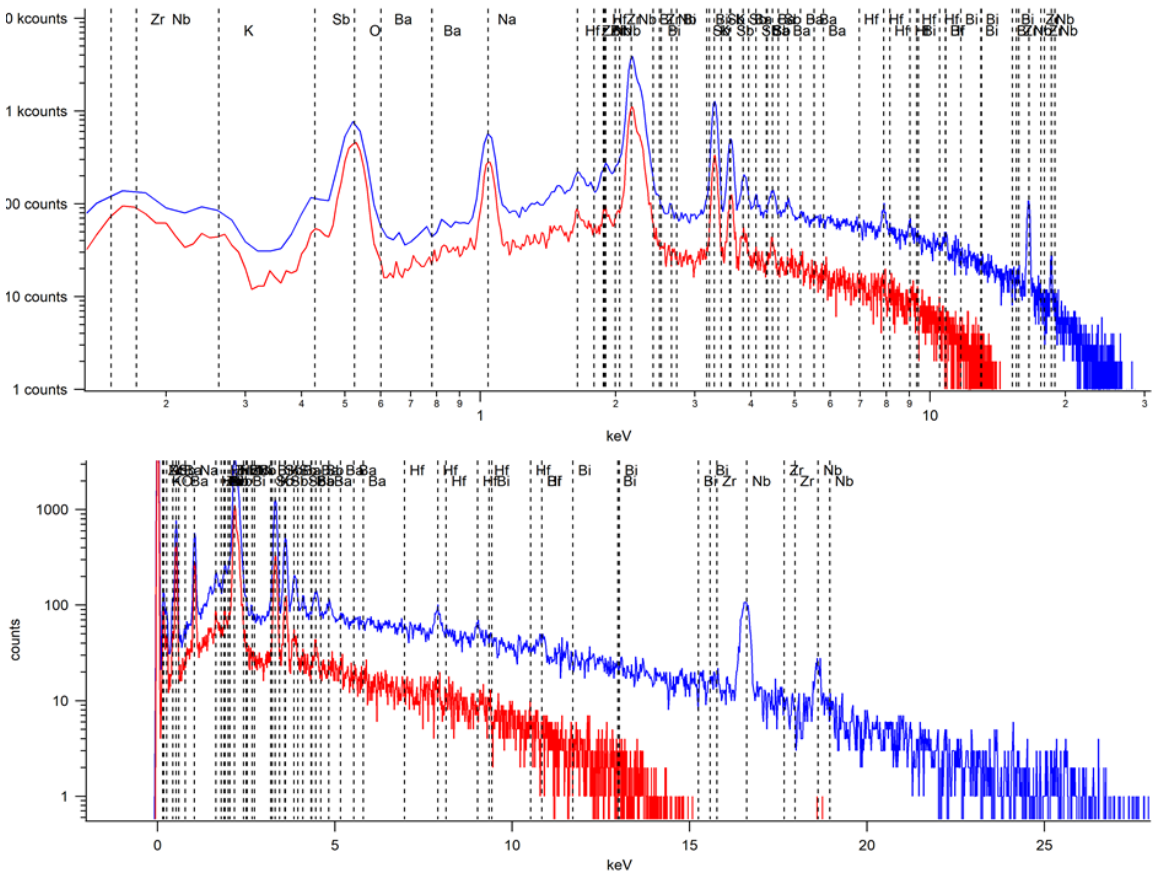

Fig. 33 EDS spectrum under 15keV and 30keV

However, in the actual use of EDS, we found that even if the ground powder samples and pre-drying methods are used, detection errors are still unavoidable. Figure 33 shows the elemental analysis pattern obtained in two modes (15 and 30keV) at the same point of the same sample: red is 15keV, blue is 30keV, and the results obtained in the two modes are very different.

By comparing and analyzing the above figure, we can see:

1) Because the sample material $0.955K_{0.48}Na_{0.52}Nb_{0.9}Sb_{0.1}O_3$-$0.025BaZrO_3$-$0.02Bi_{0.5}K_{0.5}HfO_3$ with additive m K_2CO_3 (m is selected as 0.0, 0.0066, 0.0132, 0.0198, 0.0264, 0.033, 0.0396), the type of elements contained Many of them include both light elements such as potassium and sodium, and heavy elements such as Bi. Using a single-mode (15 or 30 keV) is easy to ignore the other, and eventually cause the mass fraction of some light or heavy elements to be different from the actual situation. Too big difference;

2) In order to solve this problem, we finally decided to select the Zr element as the anchor element, and take the Ba, Bi, Hf element mass scores under 30keV, and calculate the ratio with the mass score of the Zr element, and substitute the calculated value into the replacement 15keV data The

mass fractions of Ba, Bi, and Hf elements in, and then recalculate the mass fractions of all elements to approximate the elemental composition data of the sample [69].

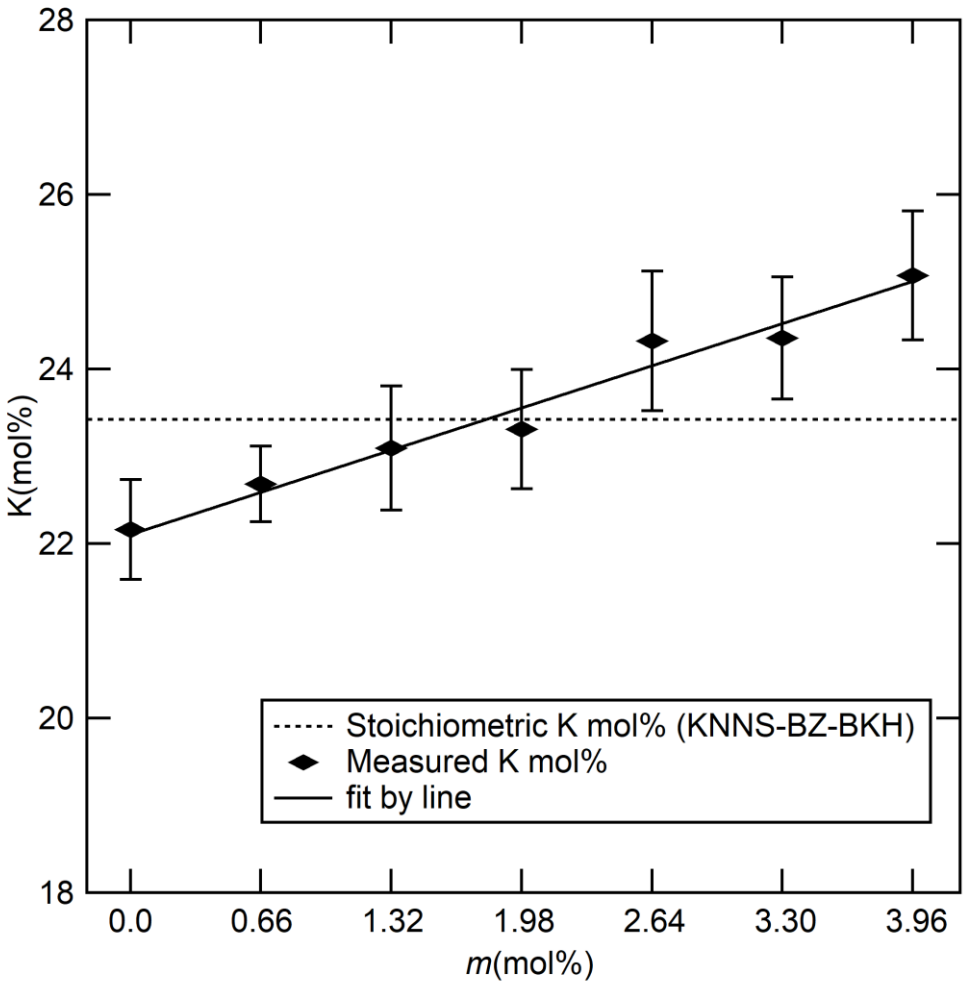

Fig. 34 The molar ratio (mol %) of potassium K with additive *m*

To optimize the element mol ratio of the material, take the EDS result at first (Table 1):

Table 1 designed and EDS result comparison

m	Na	K	Zr	Nb	Sb	Ba	Hf	Bi
0(designed)	24.83	23.42	1.25	42.98	4.78	1.25	1.00	0.50
0	22.83	22.16	1.34	44.47	5.11	1.41	1.84	0.84
0.0066(designed)	24.67	23.92	1.24	42.69	4.74	1.24	0.99	0.50
0.0066	23.02	22.68	1.01	44.20	5.05	1.39	1.79	0.85
0.0132(designed)	24.51	24.42	1.23	42.42	4.71	1.23	0.99	0.49
0.0132	22.39	23.09	1.26	44.73	4.80	1.39	1.63	0.72

0.0198(designed)	24.35	24.91	1.23	42.14	4.68	1.23	0.98	0.49
0.0198	22.08	23.31	0.95	45.11	4.81	1.41	1.73	0.60
0.0264(designed)	24.19	25.39	1.22	41.87	4.65	1.22	0.97	0.49
0.0264	21.39	24.32	1.36	44.75	4.52	1.23	1.73	0.69
0.033(designed)	24.04	25.87	1.21	41.60	4.62	1.21	0.97	0.48
0.033	22.00	24.35	1.39	44.08	4.71	1.35	1.56	0.56
0.0396(designed)	23.88	26.34	1.20	41.34	4.59	1.20	0.96	0.48
0.0396	20.94	25.07	1.29	44.30	4.72	1.46	1.57	0.64

Figure 34 shows estimated potassium mol% (except oxygen) by SEM/EDS as additive K2CO3 (m mol %) function. The estimated potassium increased linearly in 22 to 25 mol% with varying *m*. This result shows the stoichiometric component for K around 1.98 mol% as optimal. Table 1 shows the molar ratios of Na, Zr, Nb, Ba, Hf, and Bi (mol %) estimated by EDS analysis and calculated by starting compositions as a function of K_2CO_3 additives (*m* mol %). In the case of $m = 0$, the molar ratio of each element is approximately consistent in the estimation and the calculation. However, the molar ratio of K is relatively lower as compared with other elements. Therefore, the K_2CO_3 additive effectively compensates for the lack of potassium. All elements except K were approximately independent of the K_2CO_3 additives.

4.4 Result of the properties of the pellet

4.4.1 Density and d_{33} measurement of pellet

Table 2 measurement of pellet

m (mol%)	0	1.98	2.64	3.30	3.96
d_{33}(pC/N)	35.5	18.5	75	47	31.5
ε_r	229	286	181	443	257
tan δ	0.055	0.055	0.058	0.029	0.042
Density *(*g/cm^3*)*	4.0±0.1	3.9±0.3	4.0±0.3	4.1±0.3	4.1±0.3

Table 2 shows the specimens' bulk density and piezoelectric properties sintered with (T4) temperature profile (1210°C). We faced difficulty forming the pellet and polarization due to the following reasons in our current process: (1) the pellet in the alumina crucible melted and stuck to the alumina crucible. (2) The pellet was broken into pieces due to the fragile and sparse pellets

during the polishing process. (3) The pellet could not be polarized enough due to the leak current between the electrodes. Due to these difficulties of the palletization and polarization process, the m = 0.66 mol% and 1.32 mol% samples could not be made into well-polarized pellets. Here, we investigated only the successfully made pellet according to the amount of K_2CO_3 additive (m =0, 1.98, 2.64, 3.3, and 3.96 mol %) [69].

The measured density of KNNS-BZ-BKH ceramics as a function of K_2CO_3 addition slightly increases with increasing K_2CO_3 additives. The piezoelectric charge coefficient (d_{33}) of pure KNNS-BZ-BKH ceramic without additive was 35.5 pC/N while adding K_2CO_3 m = 1.98 mol% led to a decrease of d_{33} value to almost half 18.5 pC/N despite exhibiting a better crystallinity in Fig 24. Nevertheless, d_{33} increased with additive m = 2.64 mol% to 75 pC/N, consistent with the XRD diffraction patterns for powder in Fig. 4(c) and SEM images exhibiting higher grain growth in Fig 25(b). The d_{33} values of the ceramics with additive over m= 2.64 mol% exhibited a sharp decrease due to excess of K_2CO_3 additive leading to poor crystallinity and smaller grains. The sample size of the crystal and the gaps between the grains observed in SEM images of Fig 25(b) seem to influence the piezoelectric properties strongly. All the pellets showed almost the same density, and the dielectric constant and dielectric loss did not change significantly except for m = 3.3 mol% pellets. The pellet of m = 3.3 mol% may have an unknown problem in our pelletizing process.

5. Conclusion

5.1 Summary

The material maintains the perovskite orthogonal phase structure after adding 0~3.96 mol% (3 wt%) K_2CO_3 to the KNNS-BZ-BKH ceramic. The calcination temperature of 1210°C has a significant effect on increasing the crystallinity of the mixed KNNS-BZ-BKH by increasing the reaction rate of the KNNS main phase and the secondary phase $BaZrO_3$ and $Bi_{0.5}K_{0.5}HfO_3$. With a calcination temperature of 1210℃ and a K_2CO_3 additive of 1.98~2.64 mol%, KNNS-BZ-BKH has higher crystallinity. The highest piezoelectric constant d_{33} value was 75 pC/N in the optimal addition range. Compared with the stoichiometric ratio, adding elements that quickly evaporate (such as potassium) effectively improves crystallinity and piezoelectric properties.

5.2 Perspectives

High piezoelectric constants have been achieved by adding K to KNNS-based combined with choosing optimum sintering processes and poling conditions in KNN-based ceramics. A sizeable piezoelectric coefficient is observed through the construction of the phase structure proven by XRD and SEM/EDX, which is considered a result of employing a suitable preparation method. However, the piezoelectricity of KNNS-based thin films reported until now is still lower than that of the KNNS-based bulk, which needs further investigation. Therefore, as been statistically shown that the preparation methods have played an essential part in piezoelectric properties, our perspective will be focused on various research and the establishment of a comprehensive theoretical model combined with experimental testing, which is further needed to find the origin of the high-piezoelectric performance of KNNS-based materials.

References

[1] Guler U, Sendi M.S.E, Ghovanloo, M, dual-mode passive rectifier for wide-range input power flow, IEEE 60th International Midwest Symposium on Circuits and Systems (MWSCAS), Aug. 2017.

[2] "Architectures for Vibration-Driven Micropower Generators, P. D. Mitcheson, T. C. Green, E. M. Yeatman, A. S. Holmes"

[3] Olivetti, Elsa; Jeremy Gregory; Randolph Kirchain (February 2011). "Life Cycle Impacts of Alkaline Batteries with a Focus on End-of-Life - EBPA-EU" (PDF). Massachusetts Institute of Technology, Materials Systems Lab. p. 110.

[4] "BAJ Website - Monthly battery sales statistics". Battery Association of Japan. Mar 2011.

[5] "Absatzzahlen 2008" (PDF) (in German). Interessenorganisation Batterieentsorgung.

[6] Fisher, Karen; Wallén, Erika; Laenen, Pieter Paul; Collins, Michael (18 October 2006). "Battery Waste Management Life Cycle Assessment Final Report for Publication" (PDF). Environmental Resources Management, DEFRA. p. 230.

[7] "EPBA Battery Statistics - 2000". European Portable Battery Association. 2000.

[8] "Battery Care, Use and Disposal | Duracell Batteries".

[9] Batscap - La batterie lithium métal polymère Archived 2012-08-08 at the Wayback Machine in batscap.com.

[10] "BAJ Website | Monthly battery sales statistics". Baj.or.jp.

[11] "INOBAT 2008 statistics" (PDF).

[12] "Battery Waste Management - 2006 DEFRA" (PDF).

[13] "Battery Statistics". EPBAEurope.net. European Portable Battery Association. 2000.

[14] Duff, Wilmer (1916) [1908]. A Text-Book of Physics (4th ed.). Philadelphia: P. Blakiston's Son & Co. p. 361.

[15] Williams, Henry Smith. "A History of Science Volume II, Part VI: The Leyden Jar Discovered".

[16] Keithley, Joseph F. (1999). The Story of Electrical and Magnetic Measurements: From 500 BC to the 1940s. John Wiley & Sons. p. 23. ISBN 978-0780311930.

[17] Smil (1991), p. 240.

[18] Morton, Oliver (6 September 2006). "Solar energy: A new day dawning?: Silicon Valley sunrise". Nature. 443 (7107): 19–22. Bibcode:2006Natur.443...19M.

[19] Lewis, N. S.; Nocera, D. G. (2006). "Powering the Planet: Chemical challenges in solar energy utilization" (PDF). Proceedings of the National Academy of Sciences. 103 (43): 15729–35. Bibcode:2006PNAS..10315729L. doi:10.1073/pnas.0603395103. PMC 1635072. PMID 17043226.
[20] Smil (2006), p. 12.
[21] "Renewables for Heating and Cooling" (PDF). International Energy Agency. Retrieved 13 August 2015.
[22] "The Peltier Effect and Thermoelectric Cooling". ffden-2.phys.uaf.edu.
[23] Goupil, Christophe; Ouerdane, Henni; Zabrocki, Knud; Seifert, Wolfgang; Hinsche, Nicki F.; Müller, Eckhard (2016). "Thermodynamics and thermoelectricity". In Goupil, Christophe (ed.). Continuum Theory and Modeling of Thermoelectric Elements. New York, New York, USA: Wiley-VCH. pp. 2–3. ISBN 9783527413379.
[24] Gautschi, G. (2002). Piezoelectric Sensorics: Force, Strain, Pressure, Acceleration and Acoustic Emission Sensors, Materials and Amplifiers. Springer. doi:10.1007/978-3-662-04732-3. ISBN 978-3-662-04732-3.
[25] Curie, Jacques; Curie, Pierre (1880). "Développement par compression de l'électricité polaire dans les cristaux hémièdres à faces inclinées" [Development, via compression, of electric polarization in hemihedral crystals with inclined faces]. Bulletin de la Société Minérologique de France. 3 (4): 90–93. doi:10.3406/bulmi.1880.1564.
Reprinted in: Curie, Jacques; Curie, Pierre (1880). "Développement, par pression, de l'électricité polaire dans les cristaux hémièdres à faces inclinées". Comptes Rendus (in French). 91: 294–295. Archived from the original on 2012-12-05.
See also: Curie, Jacques; Curie, Pierre (1880). "Sur l'électricité polaire dans les cristaux hémièdres à faces inclinées" [On electric polarization in hemihedral crystals with inclined faces]. Comptes Rendus (in French). 91: 383–386. Archived from the original on 2012-12-05.
[26] Lippmann, G. (1881). "Principe de la conservation de l'électricité" [Principle of the conservation of electricity]. Annales de chimie et de physique (in French). 24: 145. Archived from the original on 2016-02-08.
[27] EGERTON, L.; DILLON, DOLORES M. (September 1959). "Piezoelectric and Dielectric Properties of Ceramics in the System Potassium-Sodium Niobate". Journal of the American Ceramic Society. 42 (9): 438–442. doi:10.1111/j.1151-2916.1959.tb12971.x. ISSN 0002-7820.

[28] "DIRECTIVE 2002/95/EC OF THE EUROPEAN PARLIAMENT AND OF THE COUNCIL" (PDF). Eur-lex.europa.eu. Retrieved 3 July 2015.

[29] M. Kroutvar, Y. Ducommun, D. Heiss, et al.Optically programmable electron spin memory using semiconductor quantum dots Nature, 432 (2004), pp. 81-84.

[30]H. Tao, H.J. Wu, Y. Liu, Y. Zhang, J.G. Wu, F. Li, X. Lyv, C.L. Zhao, D.Q. Xiao, J.G. Zhu, S.J. Pennycook Ultrahigh performance in lead-free piezoceramics utilizing a relaxor slush polar state with multiphase coexistence;J. Am. Chem. Soc., 141 (2019), pp. 13987-13994.

[31] W. Liu, X. Ren.Large piezoelectric effect in Pb-free ceramics,Phys. Rev. Lett., 103 (25) (2009), Article 257602.

[32] S.T. Zhang, A.B. Kounga, E. Aulbach, W. Jo, T. Granzow, H. Ehrenberg, J. Rödel.Lead-free piezoceramics with giant strain in the system $Bi_{0.5}Na_{0.5}TiO_3$–$BaTiO_3$–$K_{0.5}Na_{0.5}NbO_3$. II. Temperature dependent properties;J. Appl. Phys., 103 (2008).

[33] Liu X, Tan X (2015) Giant strains in non-textured $(Bi_{1/2}Na_{1/2})TiO_3$-based lead-free ceramics. Adv Mater 28(3):574–579.

[34] .H. Lee, D.J. Kim, J.S. Park, S.W. Kim, T.K. Song, M.H. Kim, W.J. Kim, D. Do, I.K. Jeong ;Adv. Mater., 27 (2015), pp. 6976-6982.

[35] Yuriy Poplavko, Yuriy Yakymenko, in Functional Dielectrics for Electronics, 2020.

[36] Holler, F. James; Skoog, Douglas A. & Crouch, Stanley R. (2007). Principles of Instrumental Analysis (6th ed.). Cengage Learning. p. 9. ISBN 978-0-495-01201-6.

[37] G. Shirane, K. Suzuki;J. Phys. Soc. Jpn., 7 (1952), p. 333, 10.1143/JPSJ.7.333.

[38] B. Jaffe, R.S. Roth, S. Marzullo;J. Appl. Phys., 25 (1954), pp. 809-810, 10.1063/1.1721741.

[39] B. Jaffe, W.R. Cook, H. Jaffe;Piezoelectric Ceramics(first ed.), Academic Press, London and New York (1971), p. 371.

[40] B. Noheda, D.E. Cox, G. Shirane, J.A. Gonzalo, L.E. Cross, S.E. Park;Appl. Phys. Lett., 74 (1999), pp. 2059-2061, 10.1063/1.123756.

[41] N. Zhang, H. Yokota, A.M. Glazer, Z. Ren, D.A. Keen, D.S. Keeble, P.A. Thomas, Z.G. Ye Nat. Commun., 5 (2014), p. 5231, 10.1038/ncomms6231.

[42] E. Sawaguchi, J. Phys. Soc. Jpn. 8, 615–629 (1953).

[43] Heywang W., Lubitz K. Wersing W., Piezoelectricity: Evolution and Future of a Technology, Springer, 2008.

[44] Uchino K., The Development of Piezoelectric Materials and the New Perspective, Advanced Piezoelectric Materials, 2017.

[45] S.E. Park, T.R. Shrout; Ultrahigh strain and piezoelectric behavior in relaxor based ferroelectric single crystals;J. Appl. Phys., 82 (1997), pp. 1804-1811, 10.1063/1.365983.

[46] Kobayashi K, Doshida Y, Mizuno Y, Randall CA (2013) Possibility of cofiring a nickel inner electrode in a $(Na_{0.5}K_{0.5})NbO_3$-LiF piezoelectric actuator. Jpn J Appl Phys 52:09KD07.

[47] Nagata H, Hiruma Y, Takenaka T (2010) Electric-field-induced strain for $(Bi_{1/2}Na_{1/2})TiO_3$-based lead-free multilayer actuator. J Ceram Soc Jpn 118:726–730.

[48] Bantignies C, Filoux E, Mauchamp P, Dufait R, Thi MP, Rouffaud R, Grégoire JM,Levassort F (2013) Lead-free high-frequency linear-array transducer (30 MHz) for in vivo skin imaging. Ultrasonics Symposium (IUS), IEEE International. IEEE, pp 785–788.

[49] Ahn CW, Choi G, Kim IW, Lee J-S, Wang K, Hwang Y, Jo W (2017) Forced electrostriction by constraining polarization switching enhances the electromechanical strain properties of incipient piezoceramics. NPG Asia Mater 9:e346.

[50] Nguyen V-Q, Kang J-K, Han H-S, Lee H-Y, Jeong S-J, Ahn C-W, Kim I-W, Lee J-S (2013) Bi-based lead-free ceramic multilayer actuators using AgPd-$(Na_{0.51}K_{0.47}Li_{0.02})(Nb_{0.8}Ta_{0.2})O_3$ composite inner electrodes. Sensors Actuat A-Phys 200:107–113.

[51] Cho J-H, Park J-S, Kim S-W, Jeong Y-H, Yun J-S, Park W-I, Hong Y-W, Paik J-H (2017) Ferroelectric properties and core-shell domain structures of Fe-modified $0.77Bi_{0.5}Na_{0.5}TiO_3$-$0.23SrTiO_3$ ceramics. J Eur Ceram Soc 37:3313–3318.

[52] Yang JO, Zhu BP, Zhang Y, Chen S, Yang XF, Wei W (2015) New KNN-based lead-free piezoelectric ceramic for high-frequency ultrasound transducer applications. Appl Phys A 118:1177–1181.

[53] Sapper E, Gassmann A, Gjødvad L, Jo W, Granzow T, Rödel J (2014) Cycling stability of lead-free BNT-8BT and BNT-6BT-3KNN multilayer actuators and bulk ceramics. J Eur Ceram Soc 34:653–661.

[54] Long P, Liu X, Long X, Yi Z (2017) Dielectric relaxation, impedance spectra, piezoelectric properties of $(Ba,Ca)(Ti,Sn)O_3$ ceramics and their multilayer piezoelectric actuators.J Alloys Compd 706:234–243.

[55] Lam K, Wang X, Chan H (2006) Lead-free piezoceramic cymbal actuator. Sensors Actuat A-Phys 125:393–397.

[56] Jiang S, Liu P, Zhang X, Zhang L, Li Q, Yao J, Zeng Y, Wang Q, Zhang G (2015) Enhanced pyroelectric properties of porous $Ba_{0.67}Sr_{0.33}TiO_3$ ceramics fabricated with carbon nanotubes. J Alloy Compd 636:93–96.

[57] Yuriy Poplavko, Yuriy Yakymenko, in Functional Dielectrics for Electronics, 2020.

[58] Jung JH, Lee M, Hong J, Ding Y, Chen CY, Chou LJ, Wang ZL (2011) Lead-free $NaNbO_3$ nanowires for a high output piezoelectric nanogenerator. ACS Nano 5:10041–10046.

[59] Xue QT, Wang Z, Tian H, Huan Y, Xie QY, Yang Y, Xie D, Li C, Shu Y, Wang XH, Ren TL (2015) A record flexible piezoelectric KNN ultrafine-grained nanopowder-based nanogenerator. AIP Adv 5:017102.

[60] Shin SH, Kim YH, Lee MH, Jung JY, Nah J (2014) Hemispherically aggregated $BaTiO_3$ nanoparticle composite thin film for high-performance flexible piezoelectric nanogenerator.ACS Nano 8:2766–2773.

[61] Zhou Z, Zhou Z, Sodano HA (2014) Vertically aligned $BaTiO_3$ nanowire arrays for energy harvesting. Energy Environ Sci 7:288–296.

[62] Ni X, Wang F, Lin A, Xu Q, Yang Z, Qin Y (2013) Flexible nanogenerator based on single $BaTiO_3$ nanowire. Sci Adv Mater 5:1781–1787.

[63] Jeong CK, Kim I, Park K, Oh MH, Paik H, Hwang GT, No K, Nam YS, Lee KJ (2013) Flexible nanogenerator based on single $BaTiO_3$ nanowire flexible nanogenerator based on single $BaTiO_3$ nanowire. Sci Adv Mater 7:11016–11025.

[64] Siddiqui S, Kim D, Duy LT, Nguyen MT, Muhammad S, Yoon WS, Lee NF (2015) High-performance flexible lead-free nanocomposite piezoelectric nanogenerator for biomechanical energy harvesting and storage. Nano Energy 15:177–185.

[65] Zhang G, Liao QL, Zhang Z, Liang QJ, Zhao YL, Zheng X, Zhang Y (2016) Novel piezoelectric paper-based flexible nanogenerators composed of $BaTiO_3$ nanoparticles and bacterial cellulose. Adv Sci 3:1500257.

[66] Zhao YL, Liao QL, Zhang GJ, Zhang Z, Liang Q, Liao XQ, Zhang Y (2015) High output piezoelectric nanocomposite generators composed of oriented $BaTiO_3$ Ps@PVDF. Nano Energy 11:719–727.

[67] "Solid State Chemistry and its Applications", Anthony R. West, Wiley and Sons, 2005.

[68] "Preparative Methods in Solid State Chemistry", B. Gerand, G. Nowogrocki, J. Guenot, M. Figlarz, Academic press.

[69] "Effect of K_2CO_3 additive on crystallinity and piezoelectric properties of KNNS-BZ-BKH ceramics", LHW,Zeng , R. Benioub and K. Itaka, Journal of Ceramic Processing Research. Vol. 23, No. 1, 62-68 (2022)